MOLECULAR AND CELLULAR BIOLOGY, Mar. 2009, p. 1608–1625 Vol. 29, No. 6
0270-7306/09/$08.00+0 doi:10.1128/MCB.01339-08

TRF1 Controls Telomere Length and Mitotic Fidelity in Epithelial Homeostasis▽†

Purificacion Muñoz,[1]‡§ Raquel Blanco,[1]‡ Guillermo de Carcer,[2] Stefan Schoeftner,[1] Roberta Benetti,[1]¶ Juana M. Flores,[3] Marcos Malumbres,[2] and Maria A. Blasco[1]*

Telomeres and Telomerase Group, Molecular Oncology Program, Spanish National Cancer Centre (CNIO), 28029 Madrid, Spain[1]; Cell Division and Cancer Group, Molecular Oncology Program, Spanish National Cancer Centre (CNIO), 28029 Madrid, Spain[2]; and Animal Surgery and Medicine Department, Facultad de Veterinaria, Universidad Complutense de Madrid, 28029 Madrid, Spain[3]

Received 22 August 2008/Returned for modification 20 October 2008/Accepted 26 December 2008

TRF1 is a component of the shelterin complex at mammalian telomeres; however, a role for TRF1 in telomere biology in the context of the organism is unclear. In this study, we generated mice with transgenic TRF1 expression targeted to epithelial tissues (*K5TRF1* mice). *K5TRF1* mice have shorter telomeres in the epidermis than wild-type controls do, and these are rescued in the absence of the XPF nuclease, indicating that TRF1 acts as a negative regulator of telomere length by controlling XPF activity at telomeres, similar to what was previously described for TRF2-overexpressing mice (*K5TRF2* mice). *K5TRF1* cells also show increased end-to-end chromosomal fusions, multitelomeric signals, and increased telomere recombination, indicating an impact of TRF1 on telomere integrity, again similar to the case in *K5TRF2* cells. Intriguingly, *K5TRF1* cells, but not *K5TRF2* cells, show increased mitotic spindle aberrations. TRF1 colocalizes with the spindle assembly checkpoint proteins BubR1 and Mad2 at mouse telomeres, indicating a link between telomeres and the mitotic spindle. Together, these results demonstrate that TRF1, like TRF2, negatively regulates telomere length in vivo by controlling the action of the XPF nuclease at telomeres; in addition, TRF1 has a unique role in the mitotic spindle checkpoint.

Telomere repeat binding factor 1 (TRF1) is a component of the shelterin complex at mammalian telomeres (13, 18, 31). TRF1 is proposed to act as a negative regulator of telomere length by inhibiting telomerase activity in *cis* (1, 50, 52). In human cells, TRF1 overexpression leads to telomere shortening (1, 50), while displacement of TRF1 from telomeres using a TRF1 dominant-negative allele leads to telomere elongation (52). This role of TRF1 as a negative regulator of telomere length is proposed to be mediated by its interaction with Pot1, which together with TPP1 is proposed to regulate the access of telomerase to chromosome ends (32, 50, 56, 57). In human cells, TRF1 interacts with tankyrase 1 and 2, which poly-ADP-ribosylates TRF1, thereby controlling TRF1 binding to telomeres and regulating telomere length (12, 28, 49). TRF2, a homologue of TRF1, is also a negative regulator of telomere length in human cultured cells (1, 50). In addition, TRF2 is essential for telomere capping (11, 53). TRF2 overexpression results in telomere degradation, mediated by the TRF2-interacting XPF/ERCC1 nuclease, also involved in nucleotide excision repair (NER) (7, 17, 35, 54, 58). TRF2 overexpression in the skin of mice leads to defective NER, increased skin cancer, and premature aging (7, 35). TRF1 and TRF2 share the same architecture, characterized by a C-terminal Myb domain and a TRFH N-terminal domain (9, 14, 21). Interestingly, both proteins contain distinct binding sites for the shelterin protein Tin2, probably determining their different binding partners and functions at telomeres (14). When specifically targeted to telomeres, TRF1 overexpression releases the so-called telomere position effect, suggesting a role for TRF1 in controlling telomere silencing (30). Recently, an interaction between TRF1 and RNA polymerase II (Pol II) which seems to aid in telomere transcription was described (47). In addition, TRF1 regulates sister telomere cohesion at telomeres through post-transcriptional modification by tankyrase 1 (10, 49). TRF1 has also been shown to interact with components of the mitotic spindle, including the mitotic kinase NIMA and the spindle regulator Mad1 (40, 43). Furthermore, TRF1 has been shown to interact with microtubules and to control microtubule polymerization (40).

These different roles of TRF1 in telomere biology as well as in chromosome dynamics and genomic integrity suggest an impact of TRF1 on cancer and aging. Interestingly, TRF1 is upregulated in some human epithelial cancers (33, 41), suggesting that increased TRF1 expression may favor tumorigenesis. More recently, TRF1 was found to be altered in some cases of aplastic anemia (45), a disease characterized by premature loss of bone marrow regeneration and the presence of short telomeres. In addition, the TRF1-interacting protein Tin2 is found to be mutated in some cases of dyskeratosis congenita and Revesz syndrome, also characterized by defec-

* Corresponding author. Mailing address: Telomeres and Telomerase Group, Molecular Oncology Program, Spanish National Cancer Centre (CNIO), 28029 Madrid, Spain. Phone: 34 917328031. Fax: 34 917328028. E-mail: mblasco@cnio.es.

† Supplemental material for this article may be found at http://mcb.asm.org/.

‡ P.M. and R.B. contributed equally to this work.

§ Present address: Epigenetics and Cancer Biology Program (PEBC), Catalan Institute of Oncology (ICO), Gran Via s/n, 08907 L'Hospitalet de Llobregat, Barcelona, Spain.

¶ Present address: Laboratorio Nazionale Centro Universitario Biotecnologie (LNCIB), Area Science Park, Padriciano 99, 34012 Trieste, Italy.

▽ Published ahead of print on 5 January 2009.

tive bone marrow regeneration and the presence of short telomeres (46).

Interestingly, mice deleted for TRF1 show embryonic lethality due to unknown reasons but do not appear to have defects in telomere length maintenance or telomere capping (29), arguing that TRF1 is not involved in telomere length regulation and telomere capping, at least during the very early stages of mouse embryonic development. Similarly, mice deficient in the TRF1 regulator tankyrase also show normal telomere length and telomere capping (15, 27). The lack of viable TRF1 mouse models has prevented the study of the impact of altered TRF1 expression in normal development, cancer, and aging.

In this study, we set out to address the role of TRF1 in telomere biology by generating tissue-specific TRF1 transgenic mice. In particular, we targeted TRF1 overexpression to mouse stratified epithelia by using the keratin 5 (K5) promoter, generating *K5TRF1* mice. *K5TRF1* mice show a two- to threefold increase in the amount of TRF1 bound to telomeres, which is accompanied by a slight increase of tankyrase but not of TRF2. Augmented TRF1 abundance at telomeres results in telomere shortening in vivo, indicating that TRF1 is an essential telomere length regulator in the context of epithelial homeostasis. Furthermore, we show that similar to that previously described for *K5TRF2* mice (35), telomere shortening in *K5TRF1* mice is also mediated by the XPF nuclease, suggesting that TRF1 and TRF2 act in the same pathway of telomere length control in mammals. Finally, we show that TRF1 colocalizes with the spindle assembly checkpoint (SAC) proteins BubR1 and Mad2 at mouse telomeres and that TRF1 overexpression, but not TRF2 overexpression, results in aberrant mitotic spindles, demonstrating a specific role for TRF1 in mitosis.

MATERIALS AND METHODS

Generation and maintenance of mouse strains. The full-length mouse TRF1 cDNA was cloned downstream of bovine K5 regulatory sequences (38). After digestion with NotI, DNA was microinjected at 2 μg/μl into the pronuclei of fertilized oocytes from C57BL/6 × CBA F1 mice. Five founder mice were identified by using the K5 bovine promoter as a probe. Four mice (*K5TRF1-A* to *-D*) transmitted the transgene to the offspring. Founders were backcrossed for three to five generations onto a pure C57BL/6 background to obtain the different *K5TRF1* transgenic lines studied here. All wild-type and *K5TRF1* mice used for the analyses were littermates. *K5TRF2*/*K5TRF1* double mutant mice were obtained by crossing female *K5TRF2* mice (35) with male *K5TRF1* mice. *K5TRF1*/*XPF*$^{+/-}$ mice were generated by crossing *K5TRF1* mice with *XPF*$^{+/-}$ mice, as previously described (35). *XPF* alleles were generated as described previously (35).

All mice were generated and maintained at the Spanish National Cancer Centre under specific-pathogen-free conditions in accordance with the recommendation of the Federation of European Laboratory Animal Science Associations.

Real-time quantitative RT-PCR. Total RNA was extracted using Trizol (Invitrogen Life Technologies) from the tail and back skin of three or four age-matched (2 to 5 months old) *K5TRF1-A*, *K5TRF1-B*, *K5TRF1-C*, and *K5TRF1-D* transgenic mice as well as their corresponding wild-type controls. Reserve transcription (RT) was carried out following the manufacturer's instructions (Invitrogen Life Technologies). Real-time RT-PCR was performed as described previously (35). Primers TRF1FB (5′ TCT AAG GAT AGG CCA GAT GCC A 3′) and TRF1RB (5′ CTG AAA TCT GAT GGA GCA CGT C 3′) amplified a 186-bp fragment of mouse TRF1 cDNA. The ACTIN-F and ACTIN-R primers (35) were used in parallel RT-PCRs for actin detection. We determined the relative expression of TRF1 in each sample by calculating the $\Delta\Delta C_T$ value, which expresses the difference between the cycle threshold with the TRF1 primer pair and that with the β-actin primer pair. Each RT-PCR was repeated twice.

Telomere length analyses of skin sections. Quantitative telomere fluorescence in situ hybridization (Q-FISH) directly on skin sections was performed as previously described (35).

Isolation and culture of keratinocytes from newborn mouse skin. Primary keratinocyte cultures from newborn mice (0 to 2 days old) were obtained as previously described (35).

Telomere length analyses of isolated skin keratinocytes. (i) Q-FISH analysis. Primary keratinocytes were subjected to Q-FISH as previously described (35, 44). TFL-Telo software (59) was used to quantify the fluorescence intensity from at least 10 metaphases from each genotype.

For chromosomal aberration analysis, chromosomes were analyzed by superimposing the telomere image on the DAPI (4′,6-diamidino-2-phenylindole) image of each metaphase.

(ii) TRF analysis. One million keratinocytes were included in agarose plugs, and TRF analysis was performed as described by Blasco et al. (8).

ChIP analysis. For chromatin immunoprecipitation (ChIP) analysis, 1.5×10^6 keratinocytes were used per condition. ChIP analysis with the indicated antibodies was performed as described previously (6). In all cases, ChIP values were represented as percentages of the total input DNA, therefore correcting for differences in the numbers of telomere and centromere repeats.

Analysis of TelRNAs (or TERRAs). For analysis of telomeric RNAs (TelRNAs or TERRAs), RNA dot blot analysis was performed using different amounts of RNA (Trizol; Invitrogen) as described previously (47).

Isolation of epidermal keratinocytes from adult mice. Mice were sacrificed, and the skin from the tail and back was removed surgically by making a longitudinal incision. Adult skin keratinocytes were isolated basically as described previously (35).

Tumor induction experiments. Wild-type and *K5TRF1B* littermate mice (8 to 12 weeks old) were shaved and treated with a single dose of 20 μg of DMBA [7,12-dimethylbenz(a)anthracene] (Sigma) in 200 μl of acetone. Mice were subsequently treated twice weekly with 12.5 μg of tetradecanoyl phorbol acetate (TPA; Sigma) in 200 μl of acetone each dose for 15 weeks. The number and size of papillomas were determined and registered for each mouse weekly.

Telomere length determination for skin tumor sections. For Q-FISH, paraffin-embedded tumor (SCC) sections of the indicated genotypes obtained from the DMBA-TPA experiment were deparaffinized and hybridized with a peptide nucleic acid telomeric probe. Telomere fluorescence was determined as described previously (35). More than 420 telomere signals per squamous cell carcinoma (SCC) and at least three independent SCC per genotype were analyzed. The images were captured at a magnification of ×100, using a Leica CTR MIC microscope and a Cohu high-performance charge-coupled device camera. Telomere fluorescence was integrated using spot IOD analysis in the TFL-Telo program (kindly provided by P. Landsdorp, Terry Fox Laboratory, Vancouver, Canada) (59).

Histopathological analysis. Skin samples and other mouse tissues were recovered after mouse sacrifice, fixed in 10% buffered formalin, dehydrated, and embedded in paraffin. For histopathological analysis, 4-mm sections were deparaffinized and stained with hematoxylin and eosin according to standard procedures. Images were captured with a DP-10 digital camera in an Olympus Vanox microscope at the indicated magnifications.

ESC clonogenic assays. Five thousand keratinocytes isolated from wild-type and *K5TRF1* newborn mice were seeded onto J2-3T3 fibroblasts (10^5 per well in six-well dishes) previously treated with mitomycin C (MMC) (10 mg/ml for 2 h). Keratinocytes were grown in Cnt-02 medium at 37°C and 5% CO_2 for 2 weeks. Cells were then rinsed with phosphate-buffered saline (PBS), fixed with 10% formaldehyde, and stained with 1% rhodamine B (Sigma) to visualize colony formation. For each keratinocyte sample, epidermal stem cell (ESC) clonogenic assays were performed in triplicate. The number and size of colonies were measured for each genotype, and the average numbers of colonies obtained for different ranks of size were calculated.

Telomerase TRAP assay. Telomerase activity was measured with a modified telomere repeat amplification protocol (TRAP) as described previously (8).

Telomere recombination measurements using CO-FISH. Chromosome orientation FISH (CO-FISH) was performed as described previously (3, 7, 25), using first a $(TTAGGG)_7$ probe labeled with Cy3 and then a $(CCCTAA)_7$ probe labeled with rhodamine green (Applied Biosystems, Bedford, MA). Telomere fluorescence signals and DAPI-stained chromosome images of each metaphase were captured on a Leitz Leica DMRB fluorescence microscope.

B1-SINE Cobra analysis of global DNA methylation. Global DNA methylation levels were determined using the B1-SINE Cobra method as previously described (6).

Analysis of genomic subtelomeric DNA methylation. Methylation of subtelomeric repeats at chromosomes 1 and 2 was determined by bisulfite genomic sequencing as previously described (6). One to nine colonies were sequenced per culture.

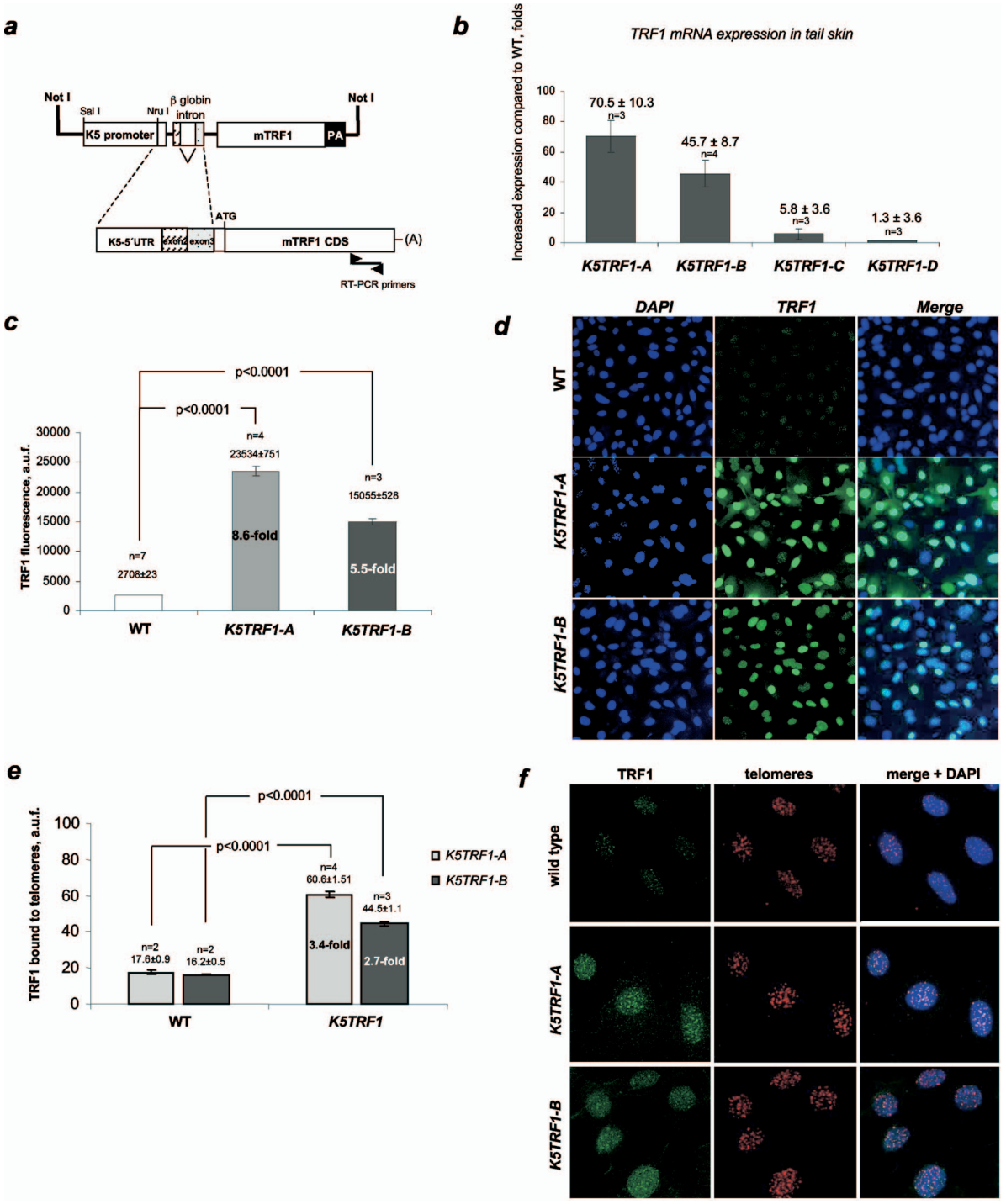

FIG. 1. Increased TRF1 expression in *K5TRF1* mice. (a) Scheme of the *K5TRF1* construct. (b) Quantification of TRF1 mRNA levels in mice from the indicated founder lines. Values represent the increases in TRF1 expression in *K5TRF1* mice compared to that in wild-type controls. The number of mice (n) and mean ± standard error (SE) are indicated above each bar. (c) Quantification of TRF1 protein levels in wild-type and *K5TRF1* primary keratinocytes by immunofluorescence. The number of keratinocyte cultures (n) and the mean ± SE are indicated above each bar. (d) Representative images of nuclear TRF1 in *K5TRF1* keratinocytes. The TRF1-specific signal is shown in green. Note the higher TRF1 immunofluorescence in *K5TRF1-A* cells than in *K5TRF1-B* cells. (e) Quantification of TRF1 protein bound to telomeres. Values are expressed as mean ± SE increases in TRF1 levels in transgenic keratinocytes relative to those in nontransgenic keratinocytes. n, number of keratinocyte cultures. (f) Representative images of telomere-bound TRF1 in the indicated genotypes. The TRF1-specific signal is shown in green, telomeric sequences detected by telomere Q-FISH are shown in red, and colocalization is shown in yellow. (g) Telomere-bound TRF2 protein is not increased in *K5TRF1* cells. Values are expressed as means ± SE relative to the wild-type level (100%). n, number of keratinocyte cultures. At least 400 TRF2 and 500 TRF1 signals were analyzed per genotype. As a control, *K5TRF2* cells showed increased TRF2 bound to telomeres compared to wild-type controls, while telomere-bound TRF1 was not increased in these cells. (h) Representative images of TRF2 and TRF1 protein levels in the indicated genotypes. (Top) TRF2 is shown in green. (Bottom) TRF1 is shown in green. (i) Increased telomere-bound tankyrase 1 protein levels in *K5TRF1* cells. Values are expressed as means ± SE relative to the wild-type level (100%). n, number of keratinocyte cultures. At least 45 nuclei were analyzed per genotype. (j) Representative images of tankyrase 1 immunofluorescence in wild-type and *K5TRF1* cells. Note the higher tankyrase 1 signal in *K5TRF1* cells.

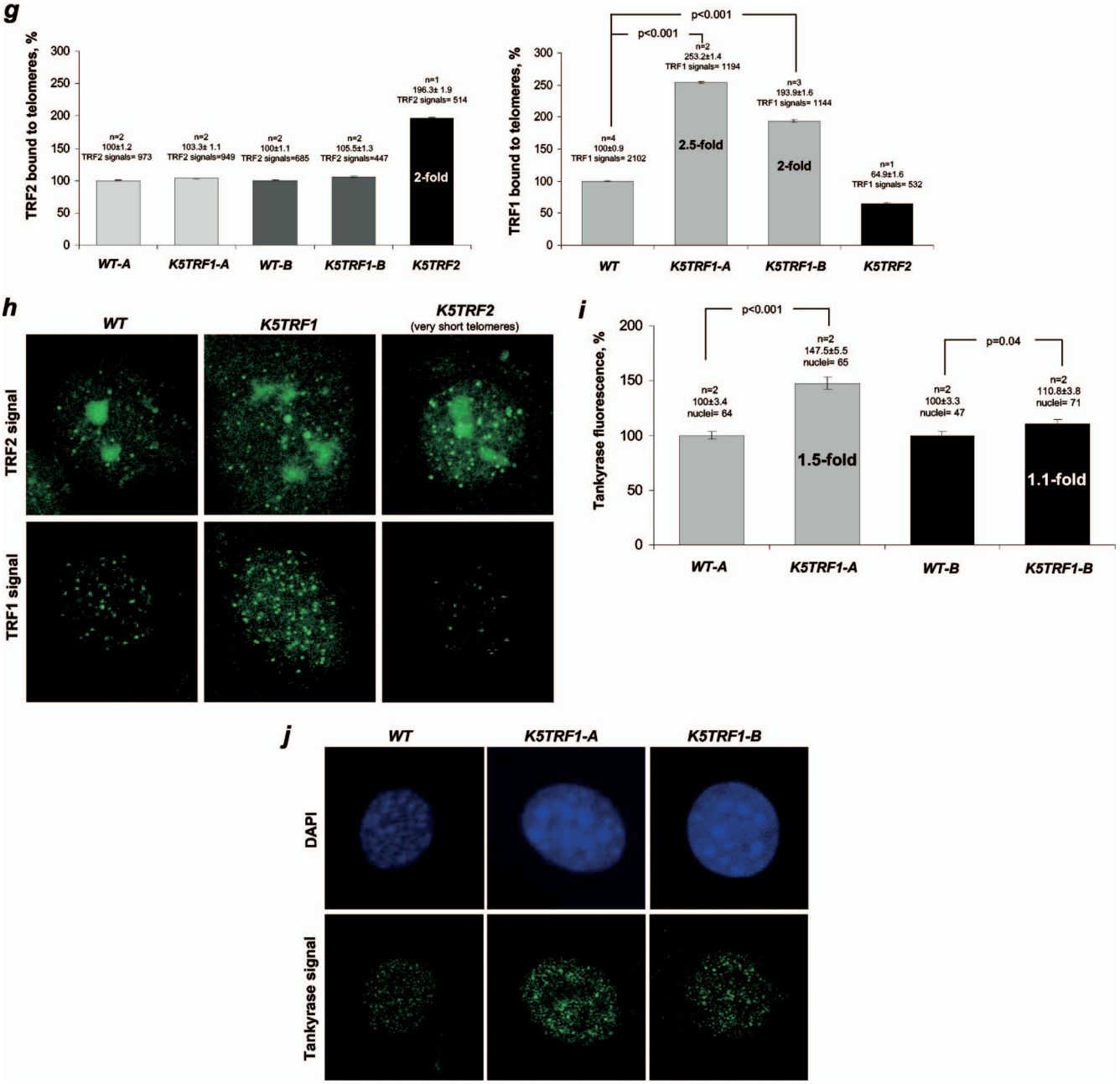

FIG. 1—*Continued.*

Antimitotic drugs and quantification of mitotic index. Primary keratinocytes were treated overnight with nocodazole (0.2 μg/ml; Sigma, St. Louis, MO) or paclitaxel (Taxol) (33 nmol; Sigma, St. Louis, MO) and fixed in PBS–buffered 4% paraformaldehyde at room temperature for 10 min, followed by permeabilization with PBS–0.1% Triton X-100 for 10 min. Cells were then blocked with 2% bovine serum albumin (Sigma, St. Louis, MO) in PBS for 1 h at room temperature and incubated for 1 h at room temperature with a rabbit anti-phospho-histone H3 (Ser10) antibody (Upstate; 1:500). After being labeled, cells were rinsed with PBS–0.1% Triton X-100 and incubated with anti-rabbit antibody–Alexa 488 (Molecular Probes), and DNA was counterstained with DAPI. The mitotic index was calculated by scoring the ratio of positive cells for phospho-histone H3.

Cytogenetic analysis. Exponentially growing primary keratinocytes were incubated with 0.1 μg/ml colcemid (Gibco) for 5 to 6 h at 37°C and then fixed with methanol-acetic acid (3:1). For analysis of chromosomal number, at least 65 metaphases per genotype were analyzed by studying the DAPI image.

Immunofluorescence. See the supplemental material for details of the different immunofluorescence experiments.

RESULTS

Transgenic mice with increased TRF1 expression in epithelial tissues. To address the role of TRF1 in telomere biology in the context of the adult organism, we targeted expression of mouse TRF1 to the basal layer and the stem cell compartments of various stratified epithelia, including the skin, by using the K5 promoter (*K5TRF1* mice) (Fig. 1a) (38). We obtained four *K5TRF1* founder mouse lines with different levels of TRF1

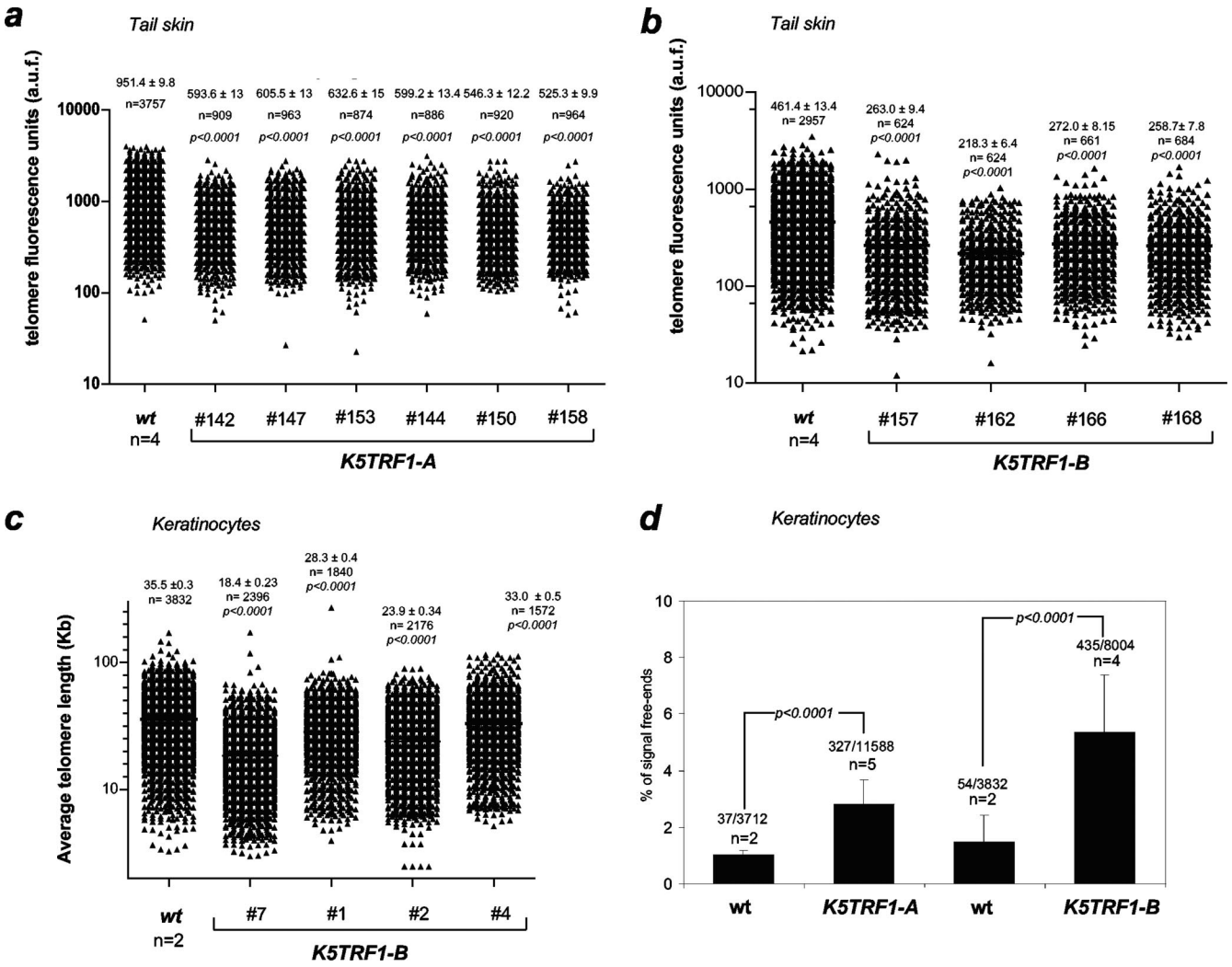

FIG. 2. Telomere shortening in *K5TRF1* mice. (a) Quantification of telomere fluorescence in tail skin sections from wild-type (wt) ($n = 4$) and *K5TRF1-A* ($n = 6$) mice. Mean ± SE telomere fluorescence (in arbitrary units) and the number of telomere dots analyzed (n) are indicated. (b) Quantification of telomere fluorescence in tail skin sections from wild-type (wt) ($n = 4$) and *K5TRF1-B* ($n = 4$) mice. Mean ± SE telomere fluorescence (in arbitrary units) and the number of telomere dots analyzed (n) are indicated. (c) Quantification of telomere length (kb) in metaphase spreads of primary keratinocytes isolated from wild-type (wt) ($n = 2$) and *K5TRF1-B* ($n = 4$) newborn mice. Mean ± SE telomere length (kb) and the number of telomeres analyzed (n) are shown. (d) The percentages of signal-free ends (telomeres with an undetectable fluorescence signal) in metaphase spreads of wild-type (wt) ($n = 2$), *K5TRF1-A* ($n = 5$), and *K5TRF1-B* ($n = 4$) primary keratinocytes are represented with bars. The number of signal-free ends of the total telomere signals analyzed per genotype is indicated above each bar. (e) Telomere length, determined by telomere restriction fragment analysis, in primary keratinocytes isolated from wild-type (wt) and *K5TRF1-B* newborn mice. Numbers at the bottom identify the cultures. Asterisks indicate keratinocyte cultures also analyzed by Q-FISH for panel c. (f) Comparison of telomere lengths determined by Q-FISH in skin sections from *K5TRF1-A* and *K5TRF1-B* mice, as well as from G1, G2, and G3 $Terc^{-/-}$ mice in a C57BL/6 genetic background. The average telomere fluorescence of each genotype is represented relative to that of the corresponding wild-type (wt) control. Telomere length values for *K5TRF1-A* and *-B* keratinocytes were obtained from panels a and b. Telomere length values for G1, G2, and G3 $Terc^{-/-}$ keratinocytes were previously described by Blanco et al. (7). Data indicating the mean ± SE and statistical significance are indicated above each bar. (g) Percentages of telomeres showing telomere fluorescence of <20% or >80% that of wild-type controls. Values were obtained as indicated for panel f.

mRNA expression in the skin (Fig. 1b). Mice from the founder line *K5TRF1-A* showed the highest TRF1 mRNA overexpression (70-fold higher than that in littermate wild-type mice), followed by *K5TRF1-B* mice (45-fold higher than that in littermate wild-type mice) (Fig. 1b). Two additional mouse founder lines, *K5TRF1-C* and *K5TRF1-D*, showed only low levels of TRF1 mRNA overexpression and were not used thereafter (Fig. 1b). In agreement with increased TRF1 mRNA levels, primary keratinocytes derived from *K5TRF1-A* and *K5TRF1-B* newborn mice showed ninefold and sixfold increases in nuclear TRF1 protein, respectively, compared with wild-type controls (Fig. 1c and d) (see Materials and Methods). To quantify TRF1 abundance specifically at telomeric regions, chromatin-unbound TRF1 was extracted before performing TRF1 immunofluorescence (see Materials and Methods). We detected 3.5-fold and 2.7-fold increased TRF1 abundances at *K5TRF1-A* and *K5TRF1-B* telomeres compared to that in wild-type controls (Fig. 1e and f; see Fig. S1 in the supplemental material for

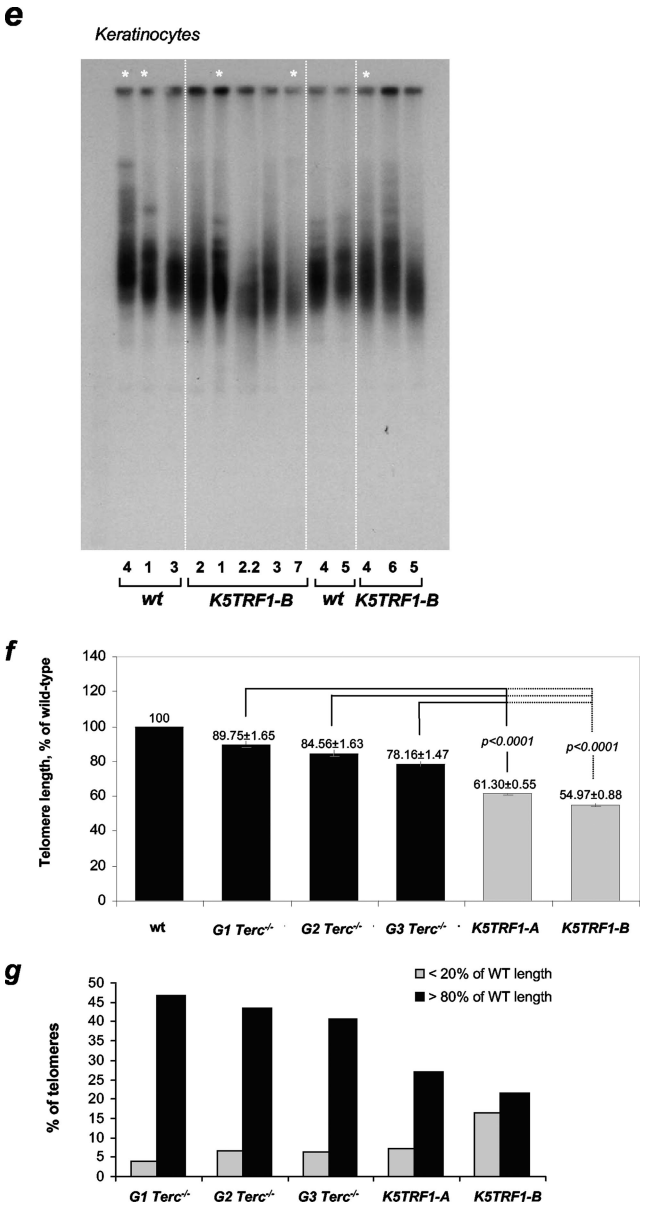

FIG. 2—*Continued.*

representative images of colocalization of TRF1 with telomeres). A similar, twofold increase in TRF1 density at *K5TRF1-A* telomeres was detected by using telomere ChIP assays (see Fig. S2a in the supplemental material). Of interest, the densities of histone 3 lysine 9 trimethylation (H3K9-3m) and H3K9 acetylation (AcH3K9) marks at telomeres were not significantly altered in *K5TRF1-A* mice compared to wild-type controls after normalization by both H3 abundance and input of telomeric DNA (see Fig. S2a in the supplemental material). Both global DNA methylation, measured by DNA methylation of SINE repeats (see Fig. S2b in the supplemental material), and subtelomeric DNA methylation, as determined by bisulfite sequencing of subtelomeric regions in chromosomes 1 and 2 (see Fig. S2c in the supplemental material), were not altered by TRF1 overexpression. This indicates that increased TRF1 density at telomeres does not significantly alter the assembly of these heterochromatic marks.

Importantly, the abundance of TRF2 at telomeres was not altered by TRF1 overexpression, as indicated both by ChIP analysis (see Fig. S2a in the supplemental material) and by TRF2 immunofluorescence (Fig. 1g and h). TRF1 immunofluorescence was increased two- to threefold in the same *K5TRF1* cells tested for TRF2 expression. As expected, TRF2 immunofluorescence was increased (twofold compared to that in wild-type controls) in cells derived from *K5TRF2* mice (Fig. 1g and h) (35). Of interest, telomere-bound TRF1 was decreased in *K5TRF2* cells (Fig. 1g and h), maybe as a consequence of very short telomeres in these cells (35). Interestingly, we also detected a significant increase in telomere-bound tankyrase 1 in both *K5TRF1-A* and *K5TRF1-B* transgenic lines (Fig. 1i and j), indicating that TRF1 overexpression results in increased loading of tankyrase 1 at mouse telomeres (see Discussion) (49). Taken together, these results indicate a two- to threefold increase in TRF1 abundance at *K5TRF1* telomeres, accompanied by an increase of telomere-bound tankyrase 1 but not of TRF2.

Telomere shortening in *K5TRF1* epidermis. Next, we addressed whether a two- to threefold increase in TRF1 abundance at telomeres was sufficient to impact telomere length in the context of skin homeostasis. For this purpose, we measured telomere length directly in *K5TRF1* tail skin sections by using Q-FISH (see Materials and Methods). Adult *K5TRF1* mice (2 to 4 months old) from the *K5TRF1-A* and *K5TRF1-B* lines showed significantly shorter telomeres than the corresponding age-matched wild-type controls ($P < 0.0001$ for all comparisons) (Fig. 2a and b). These results were confirmed by conventional metaphase Q-FISH analysis of primary keratinocytes freshly isolated from newborn *K5TRF1* and wild-type mice (Fig. 2c and d), as well as by telomere restriction fragment analysis, an independent technique based on Southern blotting (Fig. 2e). In agreement with shorter telomeres in *K5TRF1* mice, we also detected a significant increase in signal-free ends (telomeres with undetectable fluorescence by Q-FISH) in both *K5TRF1* mouse lines compared to their corresponding wild-type controls (Fig. 2d). Taken together, these results indicate that a two- to threefold increase in the amount of TRF1 bound to telomeres is sufficient to induce a significant telomere shortening in vivo, arguing for an important role for TRF1 in telomere length control in the context of epithelial homeostasis.

For illustrative purposes, we compared telomere length in the skin of *K5TRF1* mice from both founder lines to that of first- to third-generation (G1-G3) telomerase-deficient *Terc*$^{-/-}$ mice, both in a C57BL/6 genetic background (see Materials and Methods) (23, 26). To minimize possible differences in genetic background, all values are presented relative to telomere length in the corresponding wild-type controls (100%). As shown in Fig. 2f, *K5TRF1* mice from the *K5TRF1-A* and *K5TRF1-B* lines presented shorter telomeres than G1-G3 *Terc*$^{-/-}$ mice. Furthermore, *K5TRF1* mice showed an increase in the percentage of telomeres shorter than 20% of the wild-type telomere length compared to G1-G3 *Terc*$^{-/-}$ mice (Fig. 2g). These results indicate that a two- to threefold increase in TRF1 abundance at telomeres produces a more severe and rapid telomere shortening in vivo than that pro-

duced by complete telomerase ablation in the context of G1-G3 telomerase-deficient mice.

Normal telomerase activity in *K5TRF1* mice. TRF1 is proposed to act as a telomerase inhibitor in *cis* by limiting telomerase-mediated telomere elongation (50). To address this, we measured telomerase activity in keratinocytes from *K5TRF1* and wild-type mice, using an in vitro TRAP assay (see Materials and Methods). As shown in Fig. S3 in the supplemental material, telomerase TRAP activities were similar in both genotypes, ruling out that increased TRF1 protein could be directly inhibiting the telomerase catalytic activity and in this way leading to telomere shortening. This does not exclude the possibility that TRF1 could inhibit the access of telomerase to the telomere. However, the fact that increased TRF1 abundance at *K5TRF1* telomeres had a more severe effect on telomere length than that achieved by complete telomerase ablation during three generations of *Terc*-deficient mice (Fig. 2f and g) argues that TRF1 regulates telomere length, at least in part, by telomerase-independent mechanisms (see below). These findings indicate that short telomeres in *K5TRF1* mice cannot be attributed solely to inhibition of telomerase-mediated telomere elongation by TRF1.

XPF nuclease mediates telomere shortening in *K5TRF1* epidermis. We recently described that a twofold increase in TRF2 abundance at telomeres in *K5TRF2* mice results in severe telomere shortening mediated by the XPF/ERCC1 NER nuclease (7, 35) (Fig. 1g and h). Since TRF1 and TRF2 are part of the same protein complex at telomeres (18), we next addressed whether both proteins share the same molecular pathway of telomere length regulation. To this end, we generated double-transgenic *K5TRF1*/*K5TRF2* mice. Interestingly, telomere length in double-transgenic mice was indistinguishable from that in *K5TRF2* single transgenics (Fig. 3a), arguing that both proteins are likely to be in the same genetic pathway of telomere length regulation. These results also indicate that the *K5TRF2* allele is epistatic over *K5TRF1* in inducing telomere shortening, as both proteins were similarly increased (two- to threefold) at telomeres (Fig. 1g and h). Finally, it is relevant that both *K5TRF1* and *K5TRF2* alleles are epistatic over telomerase function in controlling telomere length, as indicated by the fact that *K5TRF1* and *K5TRF2* mice showed short telomeres in spite of having an intact telomerase pathway and normal levels of telomerase catalytic activity (Fig. 3a; also see Fig. S3 in the supplemental material).

Next, we investigated whether *XPF* deficiency was sufficient to rescue telomere shortening in *K5TRF1* epidermis, similarly to that previously described for *K5TRF2* mice (35). To this end, we generated *K5TRF1*/*XPF*$^{-/-}$ mice (see Materials and Methods). As shown in Fig. 3b and c, *XPF* deficiency rescued telomere length in *K5TRF1*/*XPF*$^{-/-}$ mice to the length in wild-type and *XPF*$^{-/-}$ controls. These findings indicate that increased TRF1 abundance at telomeres leads to XPF-dependent telomere degradation, further supporting the notion that TRF1 and TRF2 are in the same genetic pathway of telomere length control in mammals.

Moderately increased chromosomal aberrations in *K5TRF1* mice. To address whether telomere shortening in *K5TRF1* mice triggered chromosomal instability in these mice, we studied chromosomal aberrations involving telomeres by using conventional telomere Q-FISH on metaphase spreads (see Materials and Methods). Karyotypic analysis of primary keratinocytes from both *K5TRF1* founder lines indicated a modest increase in the frequency of end-to-end fusions (Fig. 4a and b), suggesting that telomere shortening in TRF1 mice leads to dysfunctional telomeres (Fig. 4a and b). It is relevant to note that increased TRF1 expression also led to a significant increase in chromosome breaks and fragments, as well as other types of chromosomal aberrations previously associated with TRF2 overexpression (7, 35), such as complex chromosomal aberrations, interstitial telomeres, and multitelomeric signals. This further supports the notion that the *K5TRF1* allele partially recapitulates *K5TRF2* phenotypes. The fact that both *K5TRF1* and *K5TRF2* cells show complex chromosomal aberrations may be related to their interplay with XPF, known to be involved in NER and cross-link repair.

***K5TRF1* cells are hypersensitive to the DNA cross-linking agent MMC.** The fact that *K5TRF1* cells show a significant increase in chromosomal aberrations that are not directly associated with critically short telomeres suggests that these cells may have a global defect in DNA repair, most likely as a consequence of a genetic interaction with XPF at telomeres (Fig. 3b and c). In this regard, *K5TRF2* mice have impaired NER, as indicated by an increased sensitivity to UV irradiation and to MMC (35, 58). To specifically address the putative impact of transgenic TRF1 on NER efficiency, we studied the sensitivity of *K5TRF1-A* and *K5TRF1-B* primary keratinocytes to treatment with MMC, a DNA cross-linking agent that specifically decreases the viability of ERCC1 or XPF mutant cells but not that of cells deficient in other NER components (42). *K5TRF1-A* and *K5TRF1-B* keratinocytes showed decreased viability after treatment with low doses of MMC compared to wild-type controls (Fig. 4c). Furthermore, MMC-treated *K5TRF1* keratinocytes from both founder lines showed a higher frequency of chromosome breaks and fragments as well as other complex chromosomal aberrations than did similarly treated wild-type cells (Fig. 4d and e). These observations suggest that *K5TRF1* cells have defective repair of MMC-induced DNA cross-links in the presence of normal TRF2 levels, similar to that previously described for both *K5TRF2*- and *XPF*/*ERCC1*-deficient cells (35). As previously hypothesized for *K5TRF2* mice, increased TRF1 abundance at telomeres may overrecruit XPF to telomeres, resulting in XPF-mediated telomere shortening and suboptimal NER efficiency at nontelomeric sites (35). It is relevant that in spite of having a similar sensitivity to MMC to that of *K5TRF2* mice, *K5TRF1* mice do not show the dramatic degenerative skin phenotypes present in *K5TRF2* mice, such as severe skin hyperpigmentation, hair loss, and spontaneous cancer in skin areas exposed to the light (35). This difference can be explained by longer telomeres in *K5TRF1* mice than in *K5TRF2* mice (Fig. 3a).

Increased DNA damage foci in the skin of *K5TRF1* mice. Next, we addressed whether short telomeres and increased chromosomal instability in *K5TRF1* mice resulted in increased DNA damage in the skin of these mice. γH2AX foci have previously been shown to mark the presence of DNA double-strand breaks, including those associated with critically short/dysfunctional telomeres (16, 34, 51). We quantified the percentage of basal layer keratinocytes showing γH2AX foci in skin sections. We detected a modest increase in γH2AX-pos-

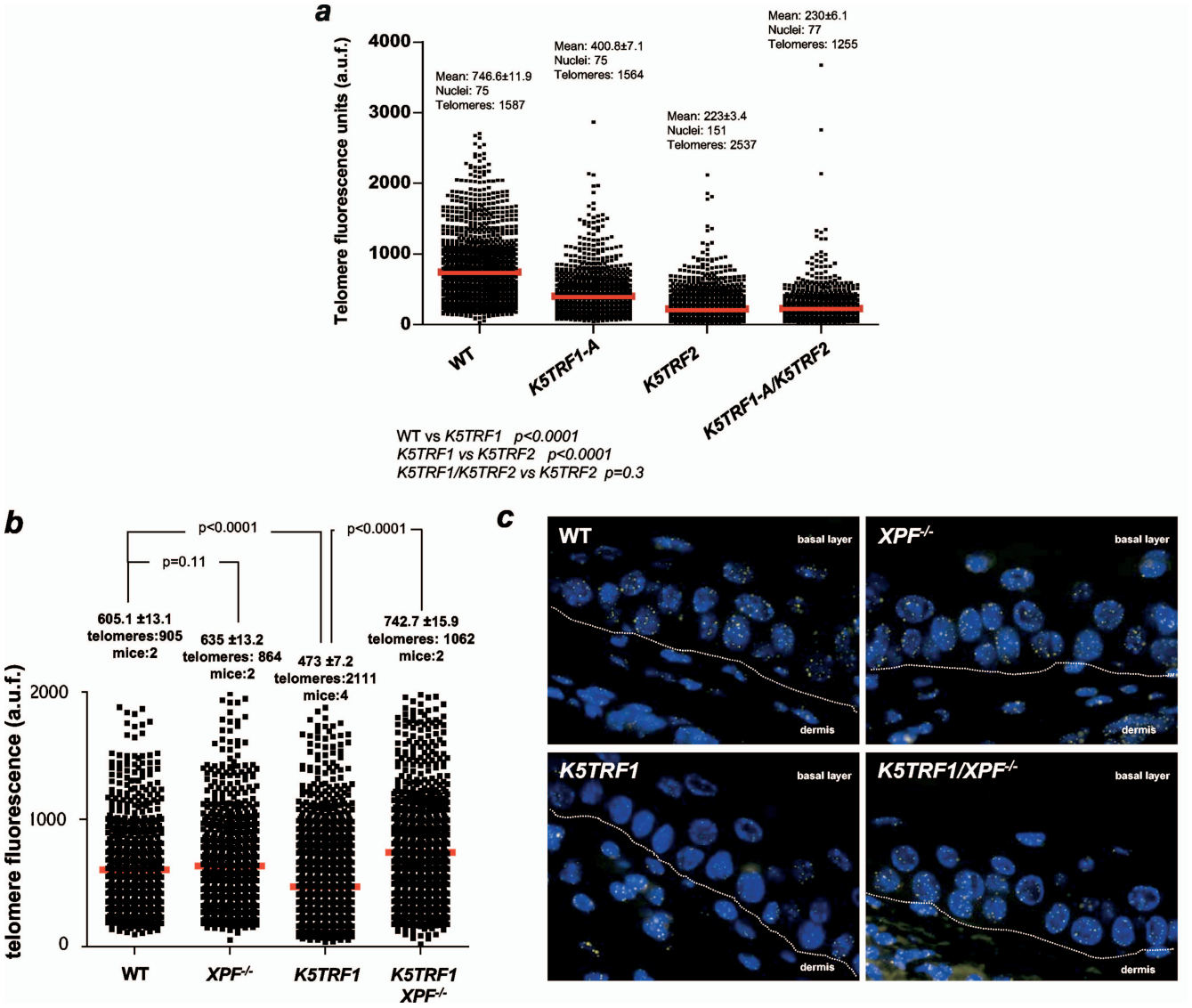

FIG. 3. XPF mediates telomere shortening in *K5TRF1* epidermis. (a) Mean ± SE telomere fluorescence (in arbitrary units) and the numbers of telomeres and nuclei used are indicated. Mean telomere length is indicated with a red bar. Note that *K5TRF1*/*K5TRF2* double-transgenic mice showed similarly short telomeres to those of *K5TRF2* mice, suggesting that the TRF2 allele is dominant over TRF1, as both proteins were similarly overexpressed (twofold) in *K5TRF1* and *K5TRF2* cells compared to their respective wild-type controls (Fig. 1g). (b) Quantification of telomere fluorescence in tail skin sections from wild-type (WT), *XPF*$^{-/-}$, *K5TRF1*, and double mutant *K5TRF1*/*XPF*$^{-/-}$ littermate mice (n = 2 to 4 mice per genotype). At least 864 telomere dots of each genotype were analyzed by Q-FISH. Average fluorescence (in arbitrary units) and SE are shown. Statistical significance is indicated in each comparison. (c) Representative images of telomere fluorescence in tail skin sections from wild-type (WT), *XPF*$^{-/-}$, *K5TRF1*, and double mutant *K5TRF1*/*XPF*$^{-/-}$ littermate mice. The dermis and basal layer are indicated and separated by a white line.

itive cells in the skin of *K5TRF1* mice compared to wild-type skin (Fig. 4f and g), suggesting that TRF1 overexpression results in a slight increase in γH2AX-positive cells in the skin of these mice, similar to that previously shown for *K5TRF2* epidermis (35).

***K5TRF1* keratinocytes show increased telomere recombination.** *K5TRF2* mice show an increased frequency of sister chromatid exchange within telomeric DNA (T-SCE) (35), suggesting a role for TRF2 in regulating homologous recombination between sister telomeric sequences (20, 36). To address this possibility in TRF1-overexpressing mice, we determined the frequency of T-SCE events in primary keratinocytes from mice with different genotypes by two-color chromosome orientation CO-FISH (3, 5). The strand-specific nature of CO-FISH typically yields two telomeric signals of each color (red, lagging strand; green, leading strand) per chromosome in the absence of recombination events. T-SCE leads to a mixture of red and green fluorescence (7, 25), detected by the leading and lagging telomere probes (Fig. 5a and b). *K5TRF1-A* and *K5TRF1-B* cells showed significantly increased T-SCE frequencies compared to wild-type cells ($P < 0.03$ in both cases) (Fig. 5a), suggesting that increased TRF1 abundance at telomeres re-

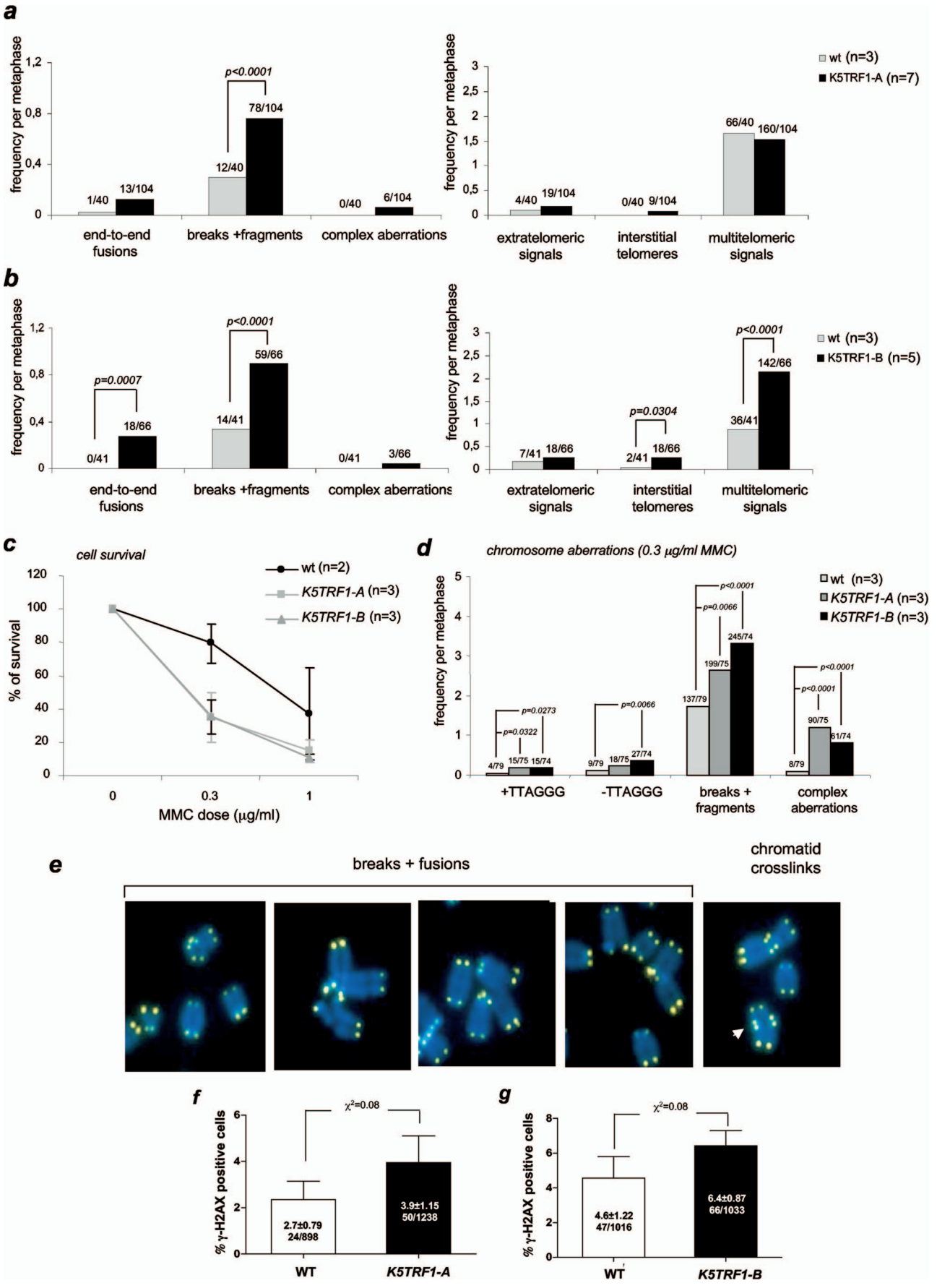
a
frequency per metaphase
1,2
0,8
0,4
0
p<0.0001
1/40
13/104
12/40
78/104
0/40
6/104
end-to-end fusions
breaks +fragments
complex aberrations
3
2,5
2
1,5
1
0,5
0
4/40
19/104
0/40
9/104
66/40
160/104
extratelomeric signals
interstitial telomeres
multitelomeric signals
wt (n=3)
K5TRF1-A (n=7)
b
p=0.0007
18/66
0/41
p<0.0001
59/66
14/41
0/41
3/66
p=0.0304
7/41
18/66
2/41
18/66
p<0.0001
142/66
36/41
wt (n=3)
K5TRF1-B (n=5)
c
cell survival
% of survival
120
100
80
60
40
20
0
0
0.3
1
MMC dose (μg/ml)
wt (n=2)
K5TRF1-A (n=3)
K5TRF1-B (n=3)
d
chromosome aberrations (0.3 μg/ml MMC)
frequency per metaphase
5
4
3
2
1
0
p=0.0273
p=0.0322
4/79
15/75
15/74
p=0.0066
9/79
18/75
27/74
p<0.0001
p=0.0066
137/79
199/75
245/74
p<0.0001
p<0.0001
8/79
90/75
61/74
+TTAGGG
-TTAGGG
breaks + fragments
complex aberrations
wt (n=3)
K5TRF1-A (n=3)
K5TRF1-B (n=3)
e
breaks + fusions
chromatid crosslinks
f
% γ-H2AX positive cells
6
4
2
0
χ²=0.08
2.7±0.79
24/898
3.9±1.15
50/1238
WT
K5TRF1-A
g
% γ-H2AX positive cells
8
6
4
2
0
χ²=0.08
4.6±1.22
47/1016
6.4±0.87
66/1033
WT
K5TRF1-B

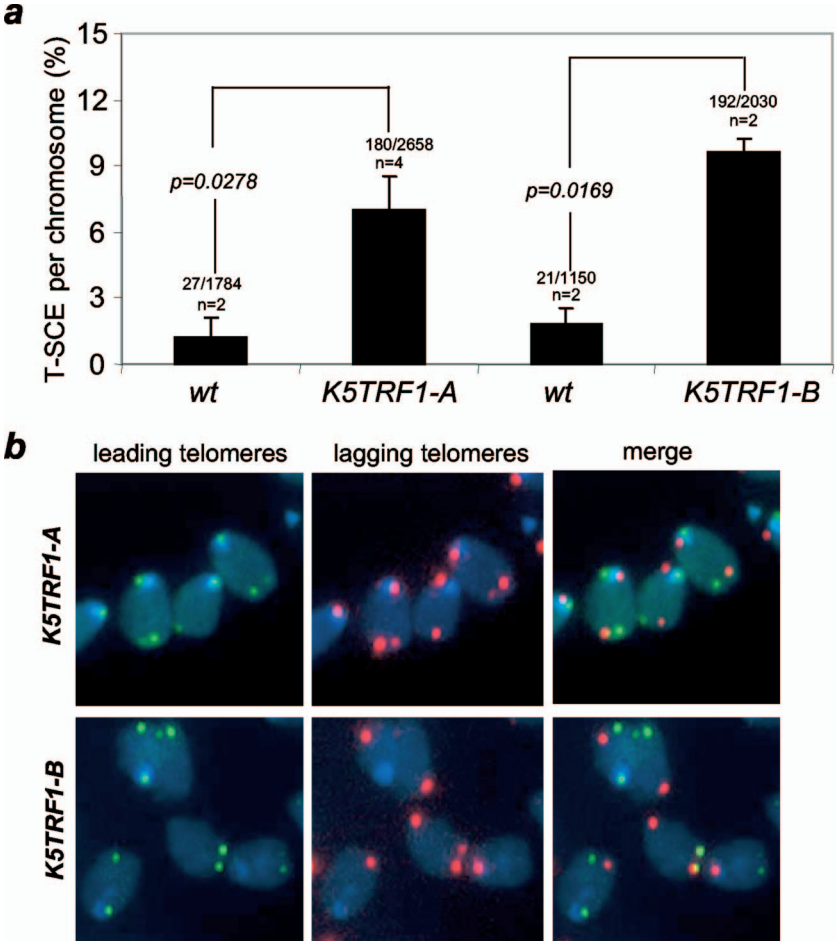

FIG. 5. Increased telomere recombination in *K5TRF1* keratinocytes. (a) Quantification of frequency of T-SCE events in wild-type (wt), *K5TRF1-A*, and *K5TRF1-B* keratinocytes analyzed by CO-FISH. The number of T-SCE events and the total number of analyzed chromosome are indicated on top of each bar. *n*, number of independent keratinocyte cultures. Statistical significance, calculated by the chi-square test, is shown. (b) Representative CO-FISH images of metaphases of the indicated genotypes hybridized with specific probes against leading (green fluorescence) and lagging (red fluorescence) telomeres.

sults in derepression of homologous recombination between sister telomeres. These results further support the notion that TRF1 and TRF2 are in a similar pathway for telomere length control. Notably, ablation of Pot1, a component of shelterin, also results in increased T-SCE frequencies (55), suggesting a more general role for shelterin in controlling DNA recombination at telomeres. We have previously shown that defects in both DNA methylation and histone trimethylation (H3K9 and H4K20 marks) are accompanied by increased T-SCE events at telomeres (6, 25), suggesting the intriguing possibility that increased TRF1 expression may indirectly affect telomere recombination by altering the status of these epigenetic marks. However, as previously discussed, we did not detect changes in global or subtelomeric DNA methylation in *K5TRF1* cells (see Fig S2b and c in the supplemental material). Similarly, we did not detect significant changes in H3K93me and AcH3K9 marks at *K5TRF1* telomeres, as determined by ChIP (see Fig. S2a in the supplemental material). Together, these results suggest that TRF1 affects telomere recombination independently of the status of these epigenetic marks.

FIG. 4. Increased chromosomal instability and MMC hypersensitivity in *K5TRF1* cells. (a and b) Quantification of chromosomal aberrations per metaphase in primary keratinocytes isolated from *K5TRF1-A* (a) and *K5TRF1-B* (b) mice. Values above each bar indicate the total number of chromosomal aberrations out of the total number of metaphases analyzed. *n*, number of independent keratinocyte cultures analyzed per genotype. (c) *K5TRF1* cells are hypersensitive to MMC treatment. Error bars represent SE. *n*, number of keratinocyte cultures used. (d) Quantification of chromosomal aberrations after MMC treatment for the indicated genotypes. The frequency of chromosomal aberrations out of the total number of metaphases analyzed is indicated above each bar. The chi-square test was used for statistical significance calculations. *n*, number of independent keratinocyte cultures examined per genotype. (e) Representative examples of the indicated chromosomal aberrations in *K5TRF1* cells. (f and g) Increased γH2AX foci in *K5TRF1* skin sections for both *K5TRF1-A* and *K5TRF1-B* founder lines. The percentage of γH2AX-positive cells per genotype is indicated. Values are expressed as means ± SE.

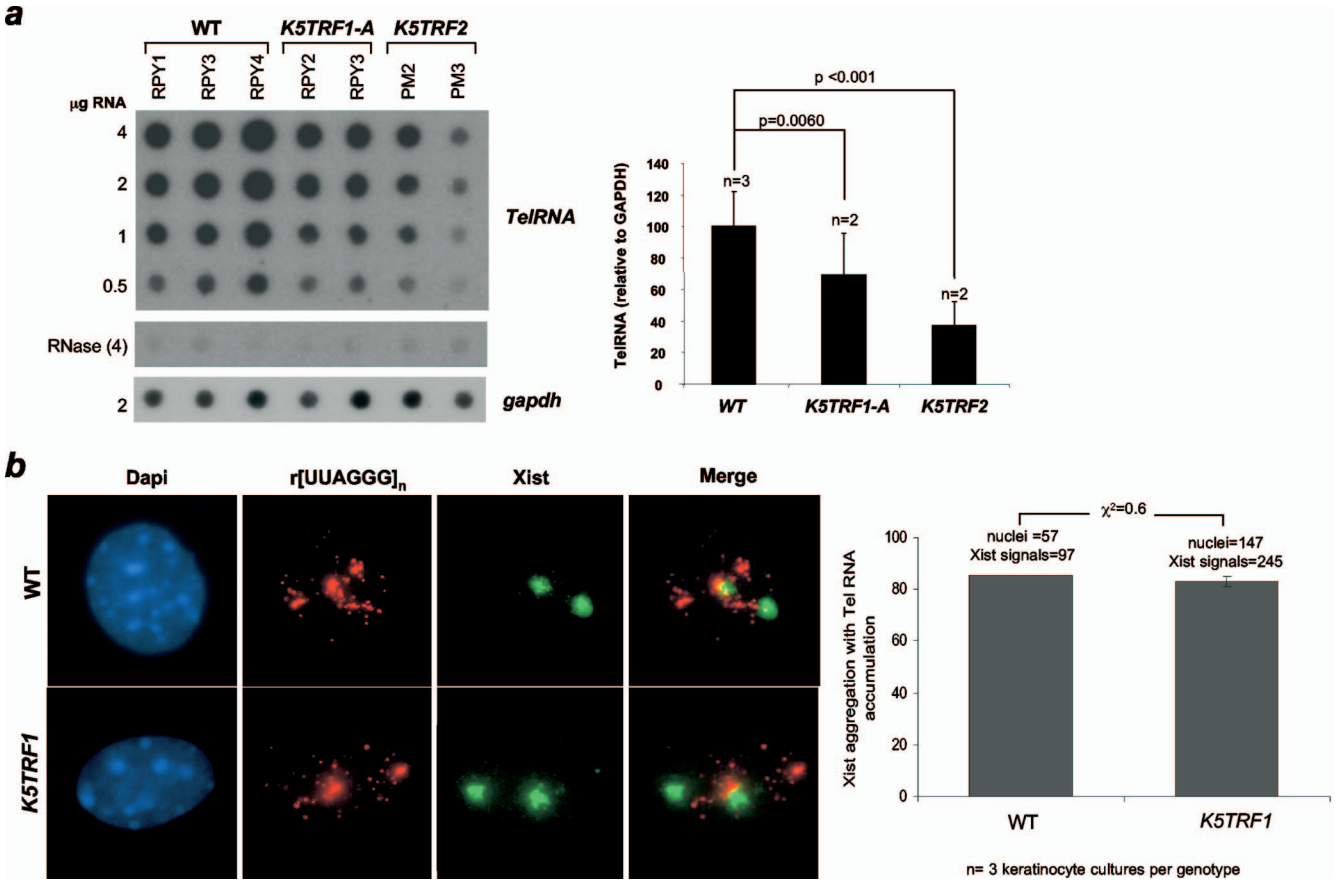

FIG. 6. Reduced telomere transcription in *K5TRF1* and *K5TRF2* cells. (a) Quantification of TelRNA levels. Average values and standard deviations were obtained for two or three independent keratinocyte cultures. GAPDH, glyceraldehyde-3-phosphate dehydrogenase. (b) Telomere RNAs accumulate near the Xist RNA marking the inactive X chromosome in both wild-type (WT) and *K5TRF1* cells.

Decreased abundance of TelRNAs (or TERRAs) associated with shorter telomeres in *K5TRF1* and *K5TRF2* mice. It was recently reported that telomeres are transcribed by the DNA-dependent RNA Pol II (47), generating long $(UUAGGG)_n$-containing RNAs that remain associated with the telomeric chromatin (2, 47). TRF1 has been proposed to support telomere transcription through direct interaction with RNA Pol II (47), and the abundance of telomere transcripts has been proposed to be proportional to the length of telomeric repeats (47). In agreement with shorter telomeres in *K5TRF1* mice, we observed decreased telomere transcription in skin keratinocytes derived from *K5TRF1* transgenic mice compared to that in wild-type controls (Fig. 6a). Furthermore, telomere transcripts in these cells showed a normal dotted nuclear distribution, including their accumulation near the inactive X chromosome in female cells (Fig. 6b). Interestingly, *K5TRF2* cells showed a further decrease in the abundance of telomere transcripts compared to *K5TRF1* mice, in agreement with the fact that *K5TRF2* cells had shorter telomeres (Fig. 6a). It is interesting that increased TRF1 occupancy of telomeres cannot rescue reduced transcription of short telomeres in *K5TRF1* keratinocytes (47). This suggests that control of telomeric transcription by telomere length is dominant over the function of TRF1 in promoting the generation of TelRNAs (47). Together, these results suggest that shorter telomeres in *K5TRF1* and *K5TRF2* mice produce fewer telomeric transcripts than do wild-type telomeres, in accordance with a positive correlation between telomere length and telomere transcription (47).

Slightly decreased clonogenic activity of *K5TRF1* ESCs. Short telomeres in telomerase-deficient mice lead to defective mobilization and clonogenic activity of ESCs, which are already noticeable at the first (G1) $Terc^{-/-}$ mouse generation (22, 48). Since *K5TRF1* mice show an important reduction in average telomere length in the skin compared to their wild-type counterparts, we set out to study the impact of TRF1 overexpression on ESCs. To this end, we determined the clonogenic activities of primary keratinocytes derived from newborn wild-type and *K5TRF1* mice (see Materials and Methods). The number and size of colonies in this assay have been proposed to reflect the ability of individual ESCs to proliferate in vitro (4). *K5TRF1* mice showed a reduced clonogenic activity compared to wild-type cells (Fig. 7), suggesting a defective ability of *K5TRF1* ESCs to proliferate and to form macroscopic colonies. This is in agreement with shorter telomeres and increased chromosomal instability in these cells.

This mild defect in ESC clonogenic activity, however, was not associated with severe skin abnormalities in *K5TRF1* mice. These results are in contrast with a dramatic impact of TRF2 overexpression on both skin aging and skin cancer (7, 35). This difference may be due to longer telomeres in *K5TRF1* cells

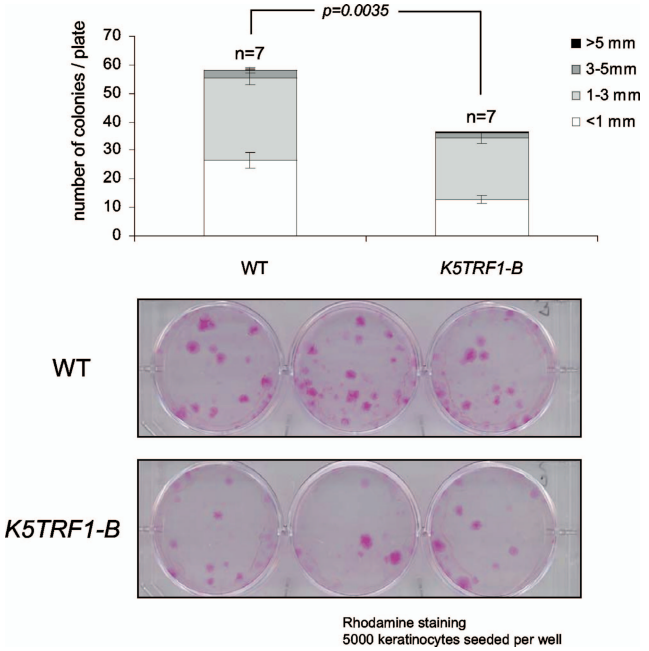

FIG. 7. Decreased clonogenic activity of *K5TRF1* ESCs. The graph shows quantification of the size and number of macroscopic colonies obtained from keratinocytes isolated from wild-type (WT) and *K5TRF1-B* newborn mice. *n*, number of independent keratinocyte cultures. Representative examples of clones obtained from the indicated genotypes are shown in the bottom panel. Clones were visualized by staining with rhodamine.

than in *K5TRF2* cells, thus highlighting the importance of short telomeres in the pathobiology of these diseases. Therefore, although both telomeric proteins are part of the same complex at telomeres, TRF2 is more potent than TRF1 in leading to dramatic telomere loss, which in turn severely impacts cancer and aging.

***K5TRF1* but not *K5TRF2* cells show aberrant mitotic spindles.** In addition to its telomeric roles, TRF1 has been suggested to be part of the mitotic spindle checkpoint (40, 43). To address whether *K5TRF1* mice showed any defects in spindle formation during mitosis, we first studied the percentage of *K5TRF1* keratinocytes showing mitotic spindle defects compared to wild-type controls. To this end, we performed confocal microscopy with TRF1 and alpha-tubulin antibodies to visualize the mitotic spindle (Fig. 8a; see Fig. S4a in the supplemental material). *K5TRF1* cells showed significantly increased mitotic spindle defects, including multipolar spindles and misaligned chromosomes, compared to wild-type controls (Fig. 8a). It is important to note that we did not find colocalization of TRF1 with microtubules (alpha-tubulin) in any of the images analyzed for either wild-type or *K5TRF1* cells (see Fig. S4a in the supplemental material). Instead, TRF1 was always located at chromosomes in all cases studied, even in cells with multipolar mitotic spindles (see Fig. S4a in the supplemental material). To analyze the specific localization of TRF1 at chromosomes, we costained TRF1 with different markers of centromeres (ACA or Aurora B), the plus end of microtubules (EB1), and the SAC proteins BubR1 and Mad2. As depicted in Fig. 8b to f, TRF1 partially colocalized with EB1, ACA, or Aurora B at the short p arms but not at the telomeric regions of the long q arms of chromosomes, probably as a consequence of the close proximity of centromeres and telomeres in murine chromosomal p arms. Similarly, the SAC regulator BubR1 colocalized with ACA and TRF1 at the p arms of the chromosomes (Fig. 8e). Interestingly, BubR1 also colocalized with TRF1 at the telomere region of the long q arms, where centromeric staining (ACA) was absent (Fig. 8e). In an analogous manner, Mad2, the critical switch of SAC activity, also colocalized with TRF1 (Fig. 8f), especially in nonaligned chromosomes, suggesting a possible link between TRF1 and deregulation of the SAC.

To specifically address this possibility, we determined the frequencies of different mitotic figures in wild-type and *K5TRF1* cells. As shown in Fig. 9a, *K5TRF1* cells displayed an abnormally high frequency of cells in prometaphase, accompanied by a decreased frequency of cells in metaphase. Furthermore, *K5TRF1* cells showed misaligned chromosomes at the metaphasic plate, abnormal spindles, and the presence of anaphase bridges (see examples in the right panel of Fig. 9a), suggesting that TRF1 overexpression results in defective mitosis. Importantly, this was not observed in *K5TRF2* cells (Fig. 9b), indicating that TRF1 overexpression, but not TRF2 overexpression, induces mitotic abnormalities and the subsequent activation of the SAC. Polyploidy was not significantly increased in cultured *K5TRF1* keratinocytes compared to the wild-type controls (see Fig. S4b in the supplemental material), suggesting that the *K5TRF1* mitotic defects cannot be attributed to increased polyploidy.

Finally, it is important to note that these mitotic defects did not result in significant functional defects in the induction of the SAC in the presence of paclitaxel or nocodazole (Fig. 9c). Similarly, *K5TRF2* cells also showed a normal sensitivity to the same mitotic poisons (Fig. 9d).

Moderately increased skin cancer and aging in *K5TRF1* mice. Since *K5TRF1* mice partially phenocopy some of the defects previously described for *K5TRF2* mice, such as XPF-mediated telomere shortening, increased end-to-end chromosome fusions, increased multitelomeric signals, increased complex chromosomal aberrations, and hypersensitivity to MMC, as well as increased telomere recombination, we next addressed whether *K5TRF1* mice also showed increased cancer susceptibility upon skin carcinogenic treatments. To this end, we treated the skin with the carcinogen DMBA, followed by weakly treatments with the tumor promoter TPA, which results in the appearance of skin papillomas and, at later times, skin carcinomas (7). As shown in Fig. S5a to c in the supplemental material, *K5TRF1* mice showed a slightly increased incidence of papilloma formation following the DMBA-plus-TPA treatment, as well as a slight increase in malignant skin tumors (SCC and BCC) (see Fig. S5c and f in the supplemental material). Interestingly, as shown in Fig. S5d in the supplemental material, we observed that TRF1 expression tended to be downregulated in DMBA-TPA-induced *K5TRF1* tumors compared to normal tissue, suggesting a selection of cells with lower TRF1 expression during tumorigenesis, something that may favor telomere elongation within the tumor. To address this, we compared the telomere lengths of three independent wild-type and *K5TRF1* SCC tumors. As shown in Fig. S5e in the supplemental material, wild-type SCC showed a quite ho-

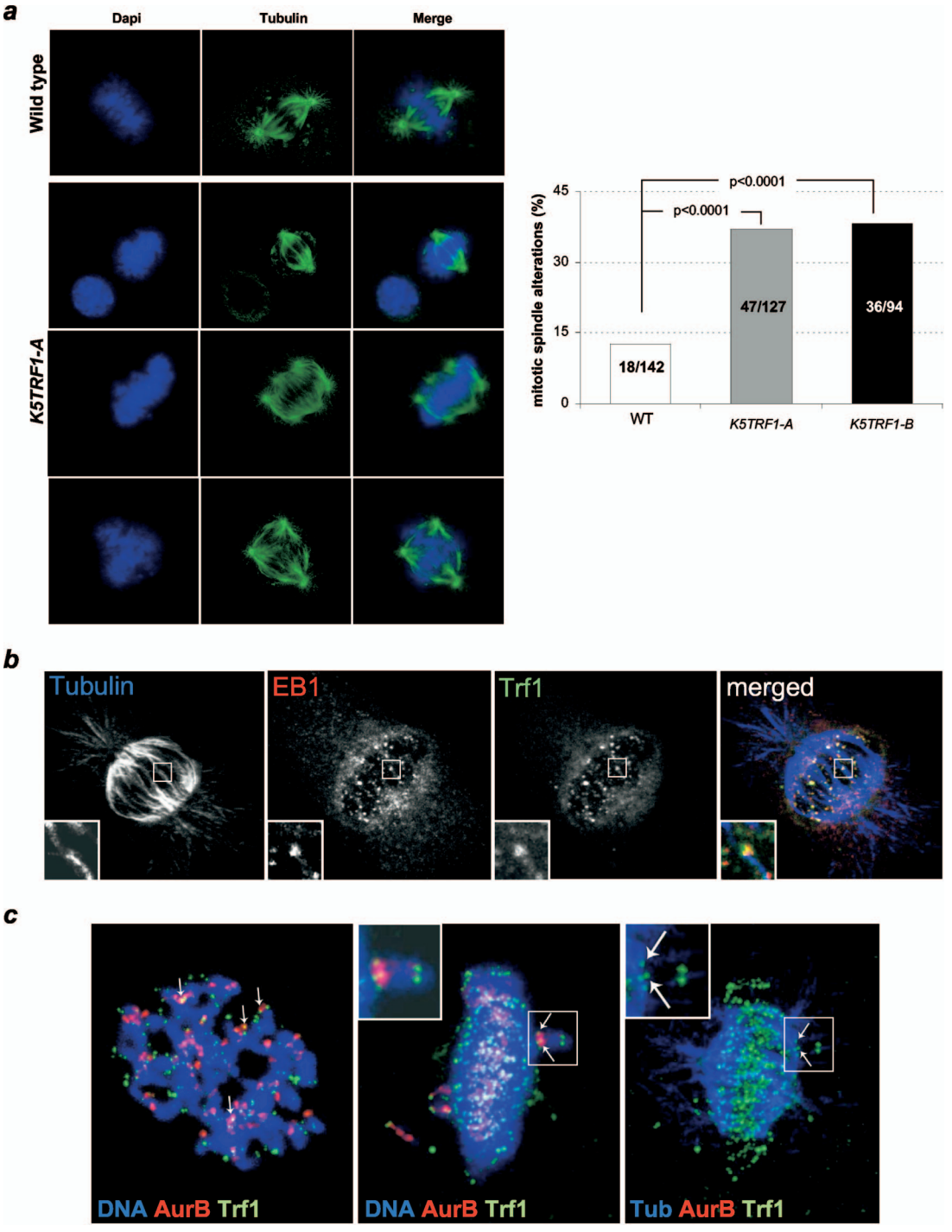

FIG. 8. TRF1 colocalizes with SAC proteins in *K5TRF1* cells. (a) Representative images of aberrant mitotic spindles in wild-type (WT) and *K5TRF1* primary keratinocytes. α-Tubulin is shown in green. The graph shows the percentages of aberrant mitotic spindles in wild-type and *K5TRF1* primary keratinocytes. The number of aberrant mitotic spindles and the total number of spindles analyzed are indicated in each bar. (b to d) TRF1 colocalizes with SAC proteins in *K5TRF1* chromosomes. Colocalization was seen between TRF1 and EB1 (plus end of microtubules close to kinetochores) (b), TRF1 and Aurora B (kinetochores) (c), and TRF1 and the centromere antigen ACA (d). (e) The SAC protein BubR1 colocalizes with TRF1 at both centromeres and p-arm telomeres (panels 2 and 3), as well as at the q-arm telomeres (panels 1 and 4), where ACA is absent. (f) Colocalization of TRF1 and Mad2. Some misaligned chromosomes (square) in *K5TRF1* keratinocytes maintain Mad2 staining that colocalizes with TRF1, not only at the p arms, where ACA is positive (arrows), but also at the q-arm telomeres, which are negative for ACA (arrowheads).

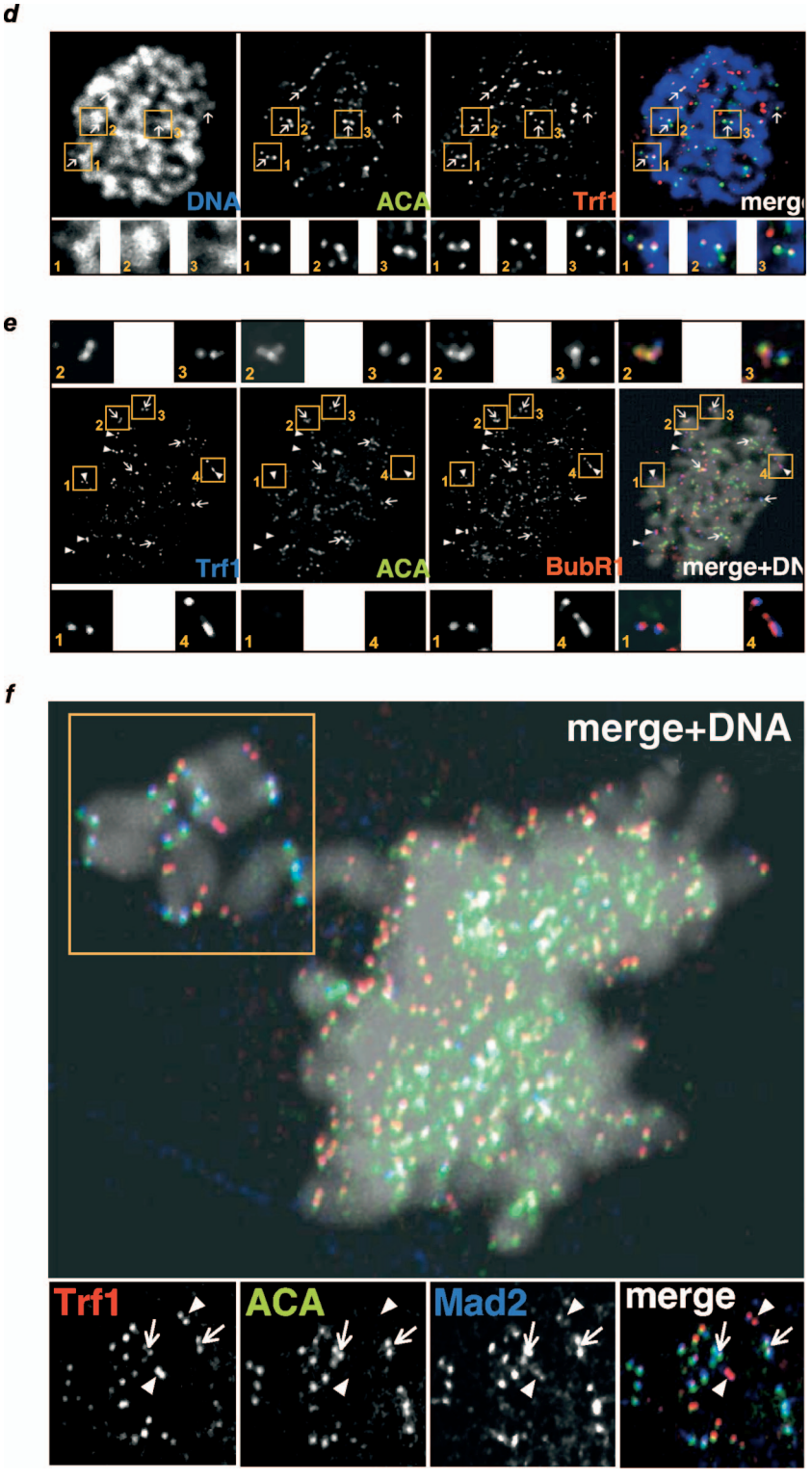

FIG. 8—*Continued.*

mogeneous telomere length whereas *K5TRF1* SCC were very heterogeneous in length, with some tumors showing very short telomeres and others showing longer telomeres than the wild-type counterparts. These results are in agreement with TRF1 overexpression leading to telomere shortening at the same time that it may favor activation of telomere recombination mechanisms. TRF1 downregulation in *K5TRF1* tumors (see Fig. S5d in the supplemental material) may also favor telomere

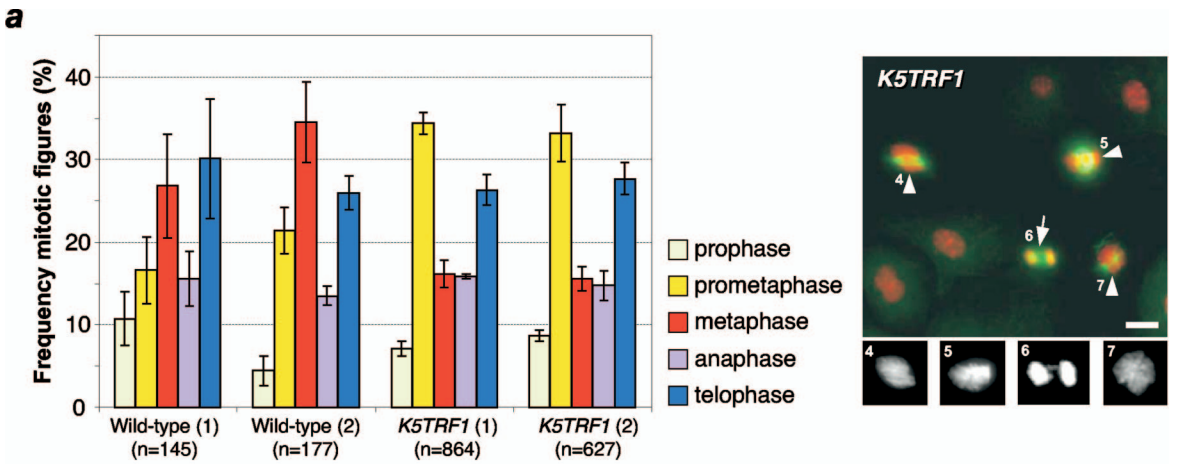
a
Frequency mitotic figures (%)
0
10
20
30
40
Wild-type (1) (n=145)
Wild-type (2) (n=177)
K5TRF1 (1) (n=864)
K5TRF1 (2) (n=627)
prophase
prometaphase
metaphase
anaphase
telophase
K5TRF1
4
5
6
7

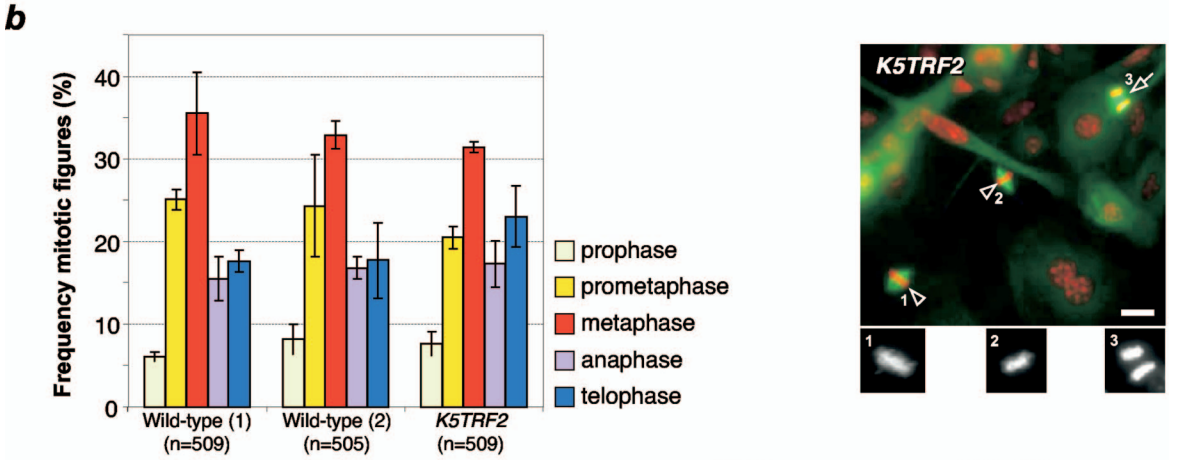
b
Frequency mitotic figures (%)
0
10
20
30
40
Wild-type (1) (n=509)
Wild-type (2) (n=505)
K5TRF2 (n=509)
prophase
prometaphase
metaphase
anaphase
telophase
K5TRF2
1
2
3

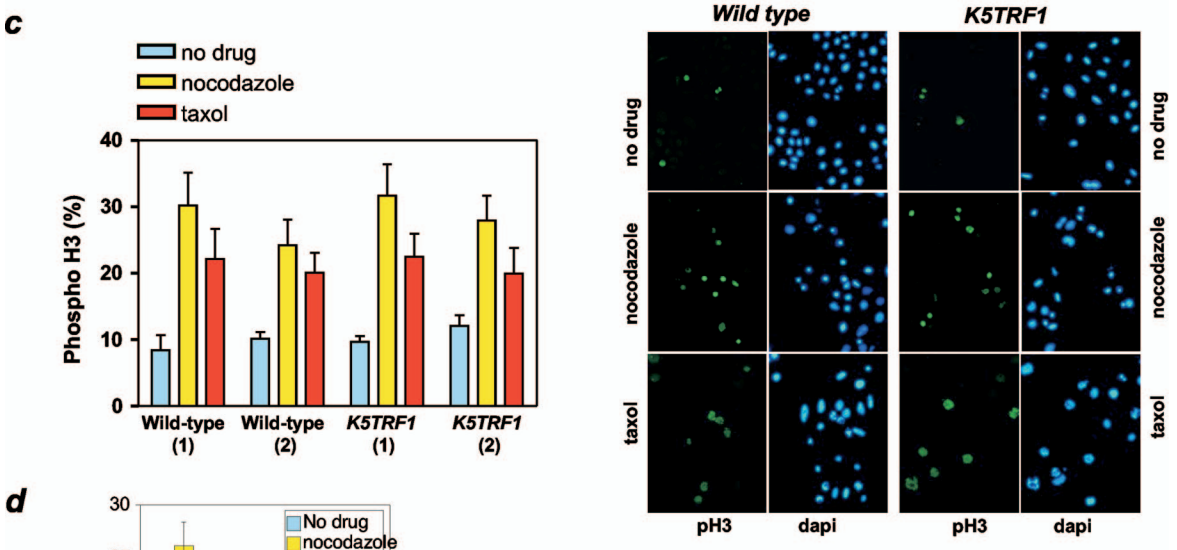
c
no drug
nocodazole
taxol
Phospho H3 (%)
0
10
20
30
40
Wild-type (1)
Wild-type (2)
K5TRF1 (1)
K5TRF1 (2)
Wild type
K5TRF1
no drug
nocodazole
taxol
pH3
dapi

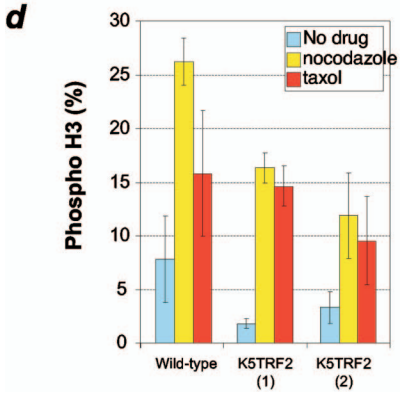
d
Phospho H3 (%)
0
5
10
15
20
25
30
No drug
nocodazole
taxol
Wild-type
K5TRF2 (1)
K5TRF2 (2)

reelongation in some of these tumors. Finally, *K5TRF1* mice showed a lifespan similar to that of wild-type mice (not shown) and a slight increase in degenerative skin lesions (atrophies, ulcers, and preneoplastic lesions) at the time of death compared to the wild-type controls (see Fig. S5g in the supplemental material), in agreement with shorter telomeres and increased DNA damage in the skin of *K5TRF1* mice.

DISCUSSION

TRF1 and its distant homologue TRF2 are central components of the shelterin complex at mammalian telomeres. Both TRF1 and TRF2 bind directly to double-stranded DNA telomeric repeats and differentially recruit to telomeres a number of additional shelterin components, as well as other telomere-interacting proteins. Mounting evidence coming from overexpression of wild-type and dominant-negative TRF1 alleles in human cultured cells suggests that TRF1 is a key regulator of telomere length (18). However, the demonstration of a role of TRF1 or its interacting factor tankyrase (12, 19, 37, 49) in telomere maintenance in the context of mammalian organisms has been lacking to date. Mice genetically ablated for TRF1 are embryonically lethal but show a normal telomere length and normal telomere protection, arguing that TRF1 is not essential for telomere length regulation in early embryonic development. Similarly, mice that lack tankyrase also show a normal telomere length and telomere capping (15, 27).

Here we show that transgenic TRF1 expression induces a significant telomere shortening in the epidermis in two independent *K5TRF1* transgenic mouse lines (*K5TRF1-A* and *K5TRF1-B*), demonstrating that a two- to threefold increase in the amount of TRF1 bound to telomeres is sufficient to provoke substantial telomere shortening in vivo. Strikingly, *K5TRF1* transgenic expression had a more severe effect on telomere length than that achieved by complete ablation of telomerase activity during three mouse generations (G1-G3 *Terc*$^{-/-}$ mice), arguing that the effects of TRF1 on telomere length are at least partially independent of telomerase activity (50). In this regard, we show here that telomere shortening provoked by TRF1 overexpression is mediated by the XPF nuclease, previously shown to be involved in degrading telomeres as a consequence of increased TRF2 expression in mice (35). Indeed, telomere phenotypes in *K5TRF1* mice are reminiscent of those previously described for *K5TRF2* mice, including telomere shortening, increased chromosomal aberrations, increased sensitivity to MMC, and increased telomere recombination, suggesting that both shelterin components may share, at least partially, the same genetic pathway of telomere length regulation. Notably, telomere shortening was considerably more severe in *K5TRF2* mice than in *K5TRF1* mice, even though both proteins were overexpressed to similar levels, indicating that TRF2 is epistatic over TRF1 in negatively regulating telomere length. Consistent with this, while TRF2 overexpression resulted in very severe degenerative skin phenotypes (hair loss, skin dryness, and hyperpigmentation), as well as spontaneous skin cancer, TRF1 transgenic mice showed only modest increases in degenerative skin lesions and chemically induced skin tumorigenesis, highlighting the importance of telomere shortening in the pathogenesis of these diseases. Finally, the fact that *K5TRF1* mice have a normal TRF2 abundance at telomeres suggests that the effects of TRF1 overexpression are not likely to be mediated indirectly by deregulated TRF2 expression in these mice. Interestingly, we observed a slight increase in tankyrase 1 binding to *K5TRF1* telomeres in spite of the fact that the acidic domain of mouse TRF1 does not bind to mouse tankyrase 1 (28), suggesting that other domains in TRF1 may recruit tankyrase 1 to mouse telomeres. Taken together, the results shown here support a model in which increased TRF1 expression results in abnormal XPF activity at telomeres, thus leading to increased telomere shortening and suboptimal NER efficiency at nontelomeric sites. Intriguingly, a direct interaction between TRF1 and NER proteins has not been found to date (58).

We recently proposed that the abundance of TelRNAs (or TERRAs) is positively correlated with the length of telomere repeats, suggesting that they may be involved in telomere length regulation (47). In agreement with this notion, *K5TRF1* mice showed a decreased abundance of telomere transcripts compared to wild-type controls, and this was further aggravated in *K5TRF2* mice, which presented even shorter telomeres.

In addition to telomere length defects in *K5TRF1* mice, we also found increased mitotic defects in cells derived from these mice. Furthermore, we found that TRF1 colocalizes with the SAC proteins BubR1 and Mad2 at mouse telomeres. In particular, *K5TRF1* cells showed a clear colocalization of TRF1 and BubR1 at both the p-arm and q-arm telomeres. In addition, Mad2, a critical regulator of SAC inactivation, also colo-

FIG. 9. Transgenic TRF1 expression induces aberrant mitotic spindles. (a) (Left) Quantification of the five different mitotic phases (prophase, prometaphase, metaphase, anaphase, and telophase). Wild-type and *K5TRF1* keratinocytes were stained for α-tubulin, phospho-histone H3, and DNA (DAPI), and mitotic cells were counted in three different experiments. *K5TRF1* cells showed an increased number of prometaphases compared to wild-type cells. (Right) *K5TRF1* cells showed dramatic mitotic aberrations, with aberrant metaphase plates (closed arrowheads) and chromosome bridges (closed arrow). Cells were stained for α-tubulin (green) and DNA (red). The bottom panels are a detailed representation of the DAPI staining. Bar, 20 μm. Numbers are for identification of individual mitoses. (b) (Left) Quantification of the five different mitotic phases (prophase, prometaphase, metaphase, anaphase, and telophase). Wild-type and *K5TRF2* keratinocytes were stained for α-tubulin, phospho-histone H3, and DNA (DAPI), and mitotic cells were counted in three different experiments. Unlike *K5TRF1* cells, *K5TRF2* cells did not show any difference from the wild-type cells. (Right) In accordance with the previous observation, *K5TRF2* metaphases were normal (open arrowheads) and anaphases did not show chromosome bridges (open arrow). Cells were stained for α-tubulin (green) and DNA (red). The bottom panels are a detailed representation of the DAPI staining. Bar, 20 μm. Numbers are for identification of individual mitoses. (c) *K5TRF1* keratinocytes display an efficient mitotic assembly checkpoint in the presence of paclitaxel (Taxol) or nocodazole. (Left) Percentages of phospho-H3-positive cells after the indicated treatments. Numbers in parentheses refer to independent keratinocyte cultures. (Right) Representative images of wild-type and *K5TRF1* phospho-H3-positive keratinocytes. (d) *K5TRF2* cells have a robust spindle assembly checkpoint. When *K5TRF2* cells were poisoned with either paclitaxel (Taxol) or nocodazole, they had a three- to fivefold increase in the mitotic index due to SAC activation.

calized with TRF1 at mouse telomeres. This is in agreement with previous findings showing a TRF1-Mad1 interaction in human cells (43). In contrast to *K5TRF1* cells, *K5TRF2* cells did not show mitotic defects, suggesting a putative role for TRF1 in spindle formation or chromosome alignment. Together, these findings suggest that an increase of TRF1 at mouse telomeres may directly or indirectly sustain the SAC response by interfering with BubR1 and Mad2. Similarly, we cannot rule out that increased tankyrase amounts at *K5TRF1* telomeres could be interfering with SAC, as tankyrase has also been proposed to regulate spindle poles (28). These results are in line with recent findings showing that BubR1 localizes to unprotected telomeres in *Drosophila* (39). It is tempting to speculate that increased TRF1 recruitment at *K5TRF1* telomeres may lead to a similar deregulation of SAC proteins and to mitotic spindle defects.

ACKNOWLEDGMENTS

M. A. Blasco's laboratory is funded by the Spanish Ministry of Innovation and Science, the Regional Government of Madrid, the European Union, and the Spanish Association Against Cancer (AECC). M. Malumbres's laboratory is funded by the Spanish Ministry of Health, the Spanish Ministry of Innovation and Science, the Consolider-Ingenio 2010 Programme (to both M.M. and M.A.B.), and the Regional Government of Madrid.

REFERENCES

1. **Ancelin, K., M. Brunori, S. Bauwens, C. E. Koering, C. Brun, M. Ricoul, J. P. Pommier, L. Sabatier, and E. Gilson.** 2002. Targeting assay to study the *cis* functions of human telomeric proteins: evidence for inhibition of telomerase by TRF1 and for activation of telomere degradation by TRF2. Mol. Cell. Biol. **22:**3474–3487.
2. **Azzalin, C. M., P. Reichenbach, L. Khoriauli, E. Giulotto, and J. Lingner.** 2007. Telomeric repeat containing RNA and RNA surveillance factors at mammalian chromosome ends. Science **318:**798–801.
3. **Bailey, S. M., M. A. Brenneman, and E. H. Goodwin.** 2004. Frequent recombination in telomeric DNA may extend the proliferative life of telomerase-negative cells. Nucleic Acids Res. **32:**3743–3751.
4. **Barrandon, Y., and H. Green.** 1987. Three clonal types of keratinocyte with different capacities for multiplication. Proc. Natl. Acad. Sci. USA **84:**2302–2306.
5. **Bechter, O. E., Y. Zou, W. Walker, W. E. Wright, and J. W. Shay.** 2004. Telomeric recombination in mismatch repair deficient human colon cancer cells after telomerase inhibition. Cancer Res. **64:**3444–3451.
6. **Benetti, R., S. Gonzalo, I. Jaco, G. Schotta, P. Klatt, T. Jenuwein, and M. A. Blasco.** 2007. Suv4-20h deficiency results in telomere elongation and derepression of telomere recombination. J. Cell Biol. **178:**925–936.
7. **Blanco, R., P. Munoz, J. M. Flores, P. Klatt, and M. A. Blasco.** 2007. Telomerase abrogation dramatically accelerates TRF2-induced epithelial carcinogenesis. Genes Dev. **21:**206–220.
8. **Blasco, M. A., H. W. Lee, M. P. Hande, E. Samper, P. M. Lansdorp, R. A. DePinho, and C. W. Greider.** 1997. Telomere shortening and tumor formation by mouse cells lacking telomerase RNA. Cell **91:**25–34.
9. **Broccoli, D., A. Smogorzewska, L. Chong, and T. de Lange.** 1997. Human telomeres contain two distinct Myb-related proteins, TRF1 and TRF2. Nat. Genet. **17:**231–235.
10. **Canudas, S., B. R. Houghtaling, J. Y. Kim, J. N. Dynek, W. G. Chang, and S. Smith.** 2007. Protein requirements for sister telomere association in human cells. EMBO J. **26:**4867–4878.
11. **Celli, G. B., and T. de Lange.** 2005. DNA processing is not required for ATM-mediated telomere damage response after TRF2 deletion. Nat. Cell Biol. **7:**712–718.
12. **Cook, B. D., J. N. Dynek, W. Chang, G. Shostak, and S. Smith.** 2002. Role for the related poly(ADP-ribose) polymerases tankyrase 1 and 2 at human telomeres. Mol. Cell. Biol. **22:**332–342.
13. **Chan, S. W., and E. H. Blackburn.** 2002. New ways not to make ends meet: telomerase, DNA damage proteins and heterochromatin. Oncogene **21:**553–563.
14. **Chen, Y., Y. Yang, M. van Overbeek, J. R. Donigian, P. Baciu, T. de Lange, and M. Lei.** 2008. A shared docking motif in TRF1 and TRF2 used for differential recruitment of telomeric proteins. Science **319:**1092–1096.
15. **Chiang, Y. J., M. L. Nguyen, S. Gurunathan, P. Kaminker, L. Tessarollo, J. Campisi, and R. J. Hodes.** 2006. Generation and characterization of telomere length maintenance in tankyrase 2-deficient mice. Mol. Cell. Biol. **26:**2037–2043.
16. **d'Adda di Fagagna, F., P. M. Reaper, L. Clay-Farrace, H. Fiegler, P. Carr, T. Von Zglinicki, G. Saretzki, N. P. Carter, and S. P. Jackson.** 2003. A DNA damage checkpoint response in telomere-initiated senescence. Nature **426:**194–198.
17. **de Laat, W. L., N. G. Jaspers, and J. H. Hoeijmakers.** 1999. Molecular mechanism of nucleotide excision repair. Genes Dev. **13:**768–785.
18. **de Lange, T.** 2005. Shelterin: the protein complex that shapes and safeguards human telomeres. Genes Dev. **19:**2100–2110.
19. **Donigian, J. R., and T. de Lange.** 2007. The role of the poly(ADP-ribose) polymerase tankyrase1 in telomere length control by the TRF1 component of the shelterin complex. J. Biol. Chem. **282:**22662–22667.
20. **Dunham, M. A., A. A. Neumann, C. L. Fasching, and R. R. Reddel.** 2000. Telomere maintenance by recombination in human cells. Nat. Genet. **26:**447–450.
21. **Fairall, L., L. Chapman, H. Moss, T. de Lange, and D. Rhodes.** 2001. Structure of the TRFH dimerization domain of the human telomeric proteins TRF1 and TRF2. Mol. Cell **8:**351–361.
22. **Flores, I., M. L. Cayuela, and M. A. Blasco.** 2005. Effects of telomerase and telomere length on epidermal stem cell behavior. Science **309:**1253–1256.
23. **Garcia-Cao, I., M. Garcia-Cao, A. Tomas-Loba, J. Martin-Caballero, J. M. Flores, P. Klatt, M. A. Blasco, and M. Serrano.** 2006. Increased p53 activity does not accelerate telomere-driven ageing. EMBO Rep. **7:**546–552.
24. Reference deleted.
25. **Gonzalo, S., I. Jaco, M. F. Fraga, T. Chen, E. Li, M. Esteller, and M. A. Blasco.** 2006. DNA methyltransferases control telomere length and telomere recombination in mammalian cells. Nat. Cell Biol. **8:**416–424.
26. **Herrera, E., E. Samper, J. Martin-Caballero, J. M. Flores, H. W. Lee, and M. A. Blasco.** 1999. Disease states associated with telomerase deficiency appear earlier in mice with short telomeres. EMBO J. **18:**2950–2960.
27. **Hsiao, S. J., M. F. Poitras, B. D. Cook, Y. Liu, and S. Smith.** 2006. Tankyrase 2 poly(ADP-ribose) polymerase domain-deleted mice exhibit growth defects but have normal telomere length and capping. Mol. Cell. Biol. **26:**2044–2054.
28. **Hsiao, S. J., and S. Smith.** 2008. Tankyrase function at telomeres, spindle poles, and beyond. Biochimie **90:**83–92.
29. **Karlseder, J., L. Kachatrian, H. Takai, K. Mercer, S. Hingorani, T. Jacks, and T. de Lange.** 2003. Targeted deletion reveals an essential function for the telomere length regulator Trf1. Mol. Cell. Biol. **23:**6533–6541.
30. **Koering, C. E., A. Pollice, M. P. Zibella, S. Bauwens, A. Puisieux, M. Brunori, C. Brun, L. Martins, L. Sabatier, J. F. Pulitzer, and E. Gilson.** 2002. Human telomeric position effect is determined by chromosomal context and telomeric chromatin integrity. EMBO Rep. **3:**1055–1061.
31. **Liu, D., M. S. O'Connor, J. Qin, and Z. Songyang.** 2004. Telosome, a mammalian telomere-associated complex formed by multiple telomeric proteins. J. Biol. Chem. **279:**51338–51342.
32. **Loayza, D., and T. De Lange.** 2003. POT1 as a terminal transducer of TRF1 telomere length control. Nature **423:**1013–1018.
33. **Matsutani, N., H. Yokozaki, E. Tahara, H. Tahara, H. Kuniyasu, K. Haruma, K. Chayama, and W. Yasui.** 2001. Expression of telomeric repeat binding factor 1 and 2 and TRF1-interacting nuclear protein 2 in human gastric carcinomas. Int. J. Oncol. **19:**507–512.
34. **Modesti, M., and R. Kanaar.** 2001. DNA repair: spot(light)s on chromatin. Curr. Biol. **11:**R229–R232.
35. **Munoz, P., R. Blanco, J. M. Flores, and M. A. Blasco.** 2005. XPF nuclease-dependent telomere loss and increased DNA damage in mice overexpressing TRF2 result in premature aging and cancer. Nat. Genet. **37:**1063–1071.
36. **Muntoni, A., and R. R. Reddel.** 2005. The first molecular details of ALT in human tumor cells. Hum. Mol. Genet. **14**(Spec. No. 2)**:**R191–R196.
37. **Muramatsu, Y., T. Ohishi, M. Sakamoto, T. Tsuruo, and H. Seimiya.** 2007. Cross-species difference in telomeric function of tankyrase 1. Cancer Sci. **98:**850–857.
38. **Murillas, R., F. Larcher, C. J. Conti, M. Santos, A. Ullrich, and J. L. Jorcano.** 1995. Expression of a dominant negative mutant of epidermal growth factor receptor in the epidermis of transgenic mice elicits striking alterations in hair follicle development and skin structure. EMBO J. **14:**5216–5223.
39. **Musaro, M., L. Ciapponi, B. Fasulo, M. Gatti, and G. Cenci.** 2008. Unprotected Drosophila melanogaster telomeres activate the spindle assembly checkpoint. Nat. Genet. **40:**362–366.
40. **Nakamura, M., X. Z. Zhou, S. Kishi, I. Kosugi, Y. Tsutsui, and K. P. Lu.** 2001. A specific interaction between the telomeric protein Pin2/TRF1 and the mitotic spindle. Curr. Biol. **11:**1512–1516.
41. **Oh, B. K., Y. J. Kim, C. Park, and Y. N. Park.** 2005. Up-regulation of telomere-binding proteins, TRF1, TRF2, and TIN2 is related to telomere shortening during human multistep hepatocarcinogenesis. Am. J. Pathol. **166:**73–80.
42. **Petit, C., and A. Sancar.** 1999. Nucleotide excision repair: from E. coli to man. Biochimie **81:**15–25.
43. **Prime, G., and D. Markie.** 2005. The telomere repeat binding protein Trf1 interacts with the spindle checkpoint protein Mad1 and Nek2 mitotic kinase. Cell Cycle **4:**121–124.

44. **Samper, E., F. A. Goytisolo, P. Slijepcevic, P. P. van Buul, and M. A. Blasco.** 2000. Mammalian Ku86 protein prevents telomeric fusions independently of the length of TTAGGG repeats and the G-strand overhang. EMBO Rep. **1:**244–252.
45. **Savage, S. A., R. T. Calado, Z. T. Xin, H. Ly, N. S. Young, and S. J. Chanock.** 2006. Genetic variation in telomeric repeat binding factors 1 and 2 in aplastic anemia. Exp. Hematol. **34:**664–671.
46. **Savage, S. A., N. Giri, G. M. Baerlocher, N. Orr, P. M. Lansdorp, and B. P. Alter.** 2008. TINF2, a component of the shelterin telomere protection complex, is mutated in dyskeratosis congenita. Am. J. Hum. Genet. **82:**501–509.
47. **Schoeftner, S., and M. A. Blasco.** 2008. Developmentally regulated transcription of mammalian telomeres by DNA-dependent RNA polymerase II. Nat. Cell Biol. **10:**228–236.
48. **Siegl-Cachedenier, I., I. Flores, P. Klatt, and M. A. Blasco.** 2007. Telomerase reverses epidermal hair follicle stem cell defects and loss of long-term survival associated with critically short telomeres. J. Cell Biol. **179:**277–290.
49. **Smith, S., I. Giriat, A. Schmitt, and T. de Lange.** 1998. Tankyrase, a poly-(ADP-ribose) polymerase at human telomeres. Science **282:**1484–1487.
50. **Smogorzewska, A., B. van Steensel, A. Bianchi, S. Oelmann, M. R. Schaefer, G. Schnapp, and T. de Lange.** 2000. Control of human telomere length by TRF1 and TRF2. Mol. Cell. Biol. **20:**1659–1668.
51. **Takai, H., A. Smogorzewska, and T. de Lange.** 2003. DNA damage foci at dysfunctional telomeres. Curr. Biol. **13:**1549–1556.
52. **van Steensel, B., and T. de Lange.** 1997. Control of telomere length by the human telomeric protein TRF1. Nature **385:**740–743.
53. **van Steensel, B., A. Smogorzewska, and T. de Lange.** 1998. TRF2 protects human telomeres from end-to-end fusions. Cell **92:**401–413.
54. **Wang, R. C., A. Smogorzewska, and T. de Lange.** 2004. Homologous recombination generates T-loop-sized deletions at human telomeres. Cell **119:**355–368.
55. **Wu, L., A. S. Multani, H. He, W. Cosme-Blanco, Y. Deng, J. M. Deng, O. Bachilo, S. Pathak, H. Tahara, S. M. Bailey, R. R. Behringer, and S. Chang.** 2006. Pot1 deficiency initiates DNA damage checkpoint activation and aberrant homologous recombination at telomeres. Cell **126:**49–62.
56. **Xin, H., D. Liu, M. Wan, A. Safari, H. Kim, W. Sun, M. S. O'Connor, and Z. Songyang.** 2007. TPP1 is a homologue of ciliate TEBP-beta and interacts with POT1 to recruit telomerase. Nature **445:**559–562.
57. **Ye, J. Z., D. Hockemeyer, A. N. Krutchinsky, D. Loayza, S. M. Hooper, B. T. Chait, and T. de Lange.** 2004. POT1-interacting protein PIP1: a telomere length regulator that recruits POT1 to the TIN2/TRF1 complex. Genes Dev. **18:**1649–1654.
58. **Zhu, X. D., L. Niedernhofer, B. Kuster, M. Mann, J. H. Hoeijmakers, and T. de Lange.** 2003. ERCC1/XPF removes the 3′ overhang from uncapped telomeres and represses formation of telomeric DNA-containing double minute chromosomes. Mol. Cell **12:**1489–1498.
59. **Zijlmans, J. M., U. M. Martens, S. S. Poon, A. K. Raap, H. J. Tanke, R. K. Ward, and P. M. Lansdorp.** 1997. Telomeres in the mouse have large inter-chromosomal variations in the number of T2AG3 repeats. Proc. Natl. Acad. Sci. USA **94:**7423–7428.